HELSINKI INSTITUTE OF PHYSICS INTERNAL REPORT SERIES

HIP - 2007 - 02

Detector Alignment Studies for the CMS Experiment

Tapio Lampén

Helsinki Institute of Physics
P.O. Box 64, FI-00014 University of Helsinki, Finland

Dissertation for the degree of Doctor of Science in Technology to be presented with due permission of the Department of Engineering Physics and Mathematics, Helsinki University of Technology, for public examination and debate in Auditorium E at Helsinki University of Technology (Espoo, Finland) on the 20th of April, 2007, at 13 o'clock.

Helsinki 2007

ISBN 978-952-10-3710-8 (printed)
ISBN 978-952-10-3711-5 (PDF)
ISSN 1455-0563

Helsinki 2007
Yliopistopaino

Acknowledgements

This thesis is based on research work carried out during the years 2000–2006 as a member of the CMS Software and Physics group of the Helsinki Institute of Physics (HIP). The work was performed initially at HIP in Helsinki, then continued at CERN during the period between September 2004 and March 2006, and then finalised in Helsinki.

I wish to express my warm thanks to *Professor Pekka Hautojärvi* for supervising my post-graduate studies and encouraging me during the writing of this thesis. I am deeply indebted to the pre-examiners *Dr. Mika Huhtinen* and *Docent Kenneth Österberg* for their thorough reading of the manuscript and for providing numerous invaluable comments.

I am grateful to *Professor Jorma Tuominiemi* for the opportunity to work in the increasingly enthusiastic atmosphere of the HIP CMS programme. I would especially like to thank my Instructor *Docent Veikko Karimäki* for his support, help and guidance during these years.

A great number of colleagues, both from HIP and CERN, have been most helpful to me in my research work. I would like to thank *Oliver Buchmüller* and *Frank-Peter Schilling*, in particular, for creating such an inspiring working atmosphere during the alignment meetings at CERN, as well as *Erkki Anttila*, *Tomas Lindén*, *Panja Luukka*, *Teppo Mäenpää* and *Lauri Wendland* for their expert comments in various issues during this work. I also want to thank the summer students of HIP — *Simo Saarinen* and *Gustav Bårdsen* — who participated in my research and to whom I had the pleasure of giving guidance.

This work has been supported financially by the *Graduate School in Particle and Nuclear Physics (GRASPANP)*, the *Magnus Ehrnrooth Foundation* and the *Waldemar von Frenckell Foundation*.

I would like to express my gratitude to all of my friends in Finland and abroad for their friendship, support and patience during this work.

Most of all, I thank my parents *Eeva* and *Pekka* and my brother *Eero* for their love and support during my whole life.

Helsinki, February 2007

Tapio Lampén

Abstract

This thesis presents studies related to track-based alignment for the future CMS experiment at CERN. Excellent geometric alignment is crucial to fully benefit from the outstanding resolution of individual sensors. The large number of sensors makes it difficult in CMS to utilize computationally demanding alignment algorithms.

A computationally light alignment algorithm, called the Hits and Impact Points algorithm (HIP), is developed and studied. It is based on minimization of the hit residuals. It can be applied to individual sensors or to composite objects. All six alignment parameters (three translations and three rotations), or their subgroup can be considered. The algorithm is expected to be particularly suitable for the alignment of the innermost part of CMS, the pixel detector, during its early operation, but can be easily utilized to align other parts of CMS also.

The HIP algorithm is applied to simulated CMS data and real data measured with a test-beam setup. The simulation studies demonstrate that the algorithm is a promising candidate for the alignment of the pixel detector. The test-beam study shows that the use of the algorithm significantly improves the data measured with genuine CMS hardware.

The positioning uncertainties of different parts of CMS have also been systematically estimated. Ready-made scenarios corresponding to these uncertainties have been implemented in the CMS reconstruction software ORCA. These scenarios have been used in the alignment studies. They have also been widely used for more realistic misalignment simulation in the physics performance studies of the CMS collaboration.

Contents

List of Publications

This thesis consists of an overview and the following publications which are referred to in the text by their Roman numerals.

I T. Lampén on behalf of the CMS collaboration, *General Alignment Concept of the CMS*, Nuclear Instruments and Methods in Physics Research A 566 (2006) 100–103

II V. Karimäki, T. Lampén, F.-P. Schilling, *Track Based Alignment of Composite Detector Structures*, IEEE Transactions on Nuclear Science 53 (6) (2006) 3830–3833

III V. Karimäki, A. Heikkinen, T. Lampén, T. Lindén, *Sensor Alignment by Tracks*, in Proceedings of 2003 Conference for Computing in High Energy and Nuclear Physics, La Jolla, California, eConf C0303241, TULT008, 6pp. (2003) [arXiv:physics/0306034]

IV T. Lampén, V. Karimäki, S. Saarinen, O. Buchmüller, *Alignment of the Cosmic Rack with the Hits and Impact Points Algorithm*, CMS Note 2006/006, CERN, Geneva, Switzerland, 8pp. (2006)

V I. Belotelov, O. Buchmüller, I. González Caballero, P. Martínez, C. Martínez-Rivero, F. Matorras, A. Heister, M. Thomas, T. Lampén, V. Valuev, *Simulation of Misalignment Scenarios for CMS Tracking Devices*, CMS Note 2006/008, CERN, Geneva, Switzerland, 12pp. (2006)

VI V. Karimäki, T. Lampén, F.-P. Schilling, *The HIP algorithm for Track Based Alignment and its Application to the CMS Pixel Detector*, CMS Note 2006/018, CERN, Geneva, Switzerland, 10pp. (2006)

VII P. Luukka, T. Lampén, L.A. Wendland, S. Czellar, E. Hæggström, J. Härkönen, V. Karimäki, I. Kassamakov, T. Mäenpää, J. Tuominiemi, E. Tuovinen, *Test Beam Results of a Proton Irradiated Czochralski Silicon Strip Detector*, Nuclear Instruments and Methods in Physics Research A 568 (2006) 72–77

Brief description of the contents of the publications

Publication I describes the general alignment strategy envisaged for the CMS experiment. The hardware alignment devices and different track-based alignment approaches of CMS are presented.

Publication II demonstrates the performance of the HIP alignment algorithm with simulated tracks in the CMS pixel detector and tracks reconstructed from experimental data recorded with a test-beam setup (CMS TOB Cosmic Rack). The CMS reconstruction software ORCA is used.

Publication III presents the performance of the HIP algorithm in a stand-alone CMS pixel detector simulation and for tracks reconstructed with experimental data from HIP Silicon Beam Telescope (SiBT). A review of other alignment methods reported in the literature is also presented.

Publication IV presents the first track-based alignment results in CMS using real data and genuine CMS hardware. The HIP and the Millepede algorithms are used with test-beam data recorded by the CMS TOB Cosmic Rack. Results are compared to manually obtained results.

Publication V presents the first estimates of the expected alignment uncertainties at different stages of the CMS operation. Software tools simulating these uncertainties are described. Examples of the impact of alignment uncertainties on the tracking performance are shown.

Publication VI presents extension of the HIP method to composite structures. Results from three alignment studies with the CMS Pixel detector are presented. The CMS reconstruction software ORCA is used.

Publication VII describes the test-beam results of a proton-irradiated microstrip detector processed on n-type magnetic Czochralski silicon. This study was carried out with the HIP Silicon Beam Telescope (SiBT).

Author's contribution

The author has had an active role in all published papers. He has collected and combined the information needed for publications I and V. For publication VII, his responsibility was to perform a detailed off-line analysis of the test-beam data. He has been developing the software tools utilized in publications II, IV, V and VI, written publications I, II and IV, and contributed to the writing process of publications III, V, VI and VII.

1 Introduction

The Large Hadron Collider (LHC) is a circular proton-proton collider scheduled to begin operation at the end of 2007 at CERN, European Organization for Nuclear Research, in Geneva, Switzerland. It will provide extraordinary prospects in particle physics with its unprecedented collision energy and luminosity. The new energy regime of the scale of 1 TeV centre-of-mass energy in the parton-parton interaction makes it possible to discover new fundamental aspects of Nature. The LHC is designed especially to discover the Higgs particle, the yet undiscovered but predicted particle of the prevailing theory of particle physics, the *Standard Model*.

According to the Standard Model, unification of the electromagnetic and the weak nuclear interaction as such to a single electroweak interaction would require all its force carrier particles to be massless. However, whereas the force carrier of electromagnetic interaction, the photon, has indeed a zero mass, the force carriers of the weak interaction, the W and Z bosons, have different respective nonzero experimentally measured masses. Because of this mass difference it is said that the *electroweak symmetry* is broken. The Higgs particle is part of a subtle mechanism that explains the mass difference by introducing *spontaneous electroweak symmetry breaking* to the Standard Model. According to this mechanism, a vacuum is filled by a scalar field (the *Higgs field*), and fermions obtain their masses by interacting with this field. The Higgs boson emerges as a result of the existence of the Higgs field. Detection of the Higgs boson would serve as direct experimental evidence of this mechanism.

Predictions of the Standard Model agree with all experimental results so far, but there are, however, good reasons to believe that it is not a complete model, but an effective theory valid below the energy scale of 1 TeV. Therefore, it should be extended by new physics, which should be detected in the LHC. Several theories beyond the Standard Model exist, and many of them are of great fundamental importance, for instance, the theories of extra dimensions and supersymmetry.

In addition to new discoveries, the LHC will also provide outstanding possibilities for precise studies of already discovered particles, for instance, the top quark discovered at Fermilab in 1995.

In the LHC, the outcome of proton-proton collisions (*events*) consists of charged particle trajectories (*tracks*) and energy deposits of both charged and neutral particles. These are measured with complex and large detector systems such as the CMS (*Compact Muon Solenoid*) [1] experiment. To make precise and reliable measurements, detectors need to be carefully geometrically calibrated. High-precision position measurements as close as possible to the collision point are particularly relevant for the identification of short-lived heavy flavour particles (b- and τ-tagging). Also, the precision of the momentum measurement depends directly on the precision of individual position measurements. To fully benefit from the excellent resolution of individual tracker sensors, their geometrical positions need to be known with an accuracy comparable to their intrinsic resolution, which is typically

of the order of tens of micrometers. As the initial installation uncertainties can be much larger than the resolution of sensors, a sophisticated *alignment process* is needed.

Alignment can be carried out with a dedicated hardware system, with reconstructed particle tracks or with both. The development of alignment methods is currently of great importance, since they will be needed in the first days of operation, possibly as soon as the end of 2007. This thesis presents studies of a track-based alignment algorithm developed for the CMS detector by the team from Helsinki Institute of Physics. The algorithm is called the *Hits and Impact Points* algorithm (HIP). It could be utilized, for instance, in the alignment of the CMS pixel detector in its early operation.

Publications in this thesis describe the HIP algorithm and its application to a simulated CMS detector. The publications also describe the software tools (*misalignment scenarios*) developed to test the algorithm. These tools have also been extensively used within the CMS collaboration for more realistic physics simulations. The application of the HIP algorithm to a test-beam setup is also described.

The general strategy for the alignment of the CMS detector is presented in publication I. The HIP algorithm is applied to the simulated CMS detector in publications II, III and VI. In publication IV, it is applied to cosmic muon data measured with genuine CMS detector modules in the Cosmic Rack installation. Results of survey measurements of the support structures carried out in Helsinki are also presented in publication IV.

Publication VII demonstrates that track-based alignment is beneficial even in a small test-beam setup. In this publication, the properties of a microstrip detector processed on a magnetic Czochralski (MCZ) grown silicon substrate were studied after a severe proton irradiation. Rigorous alignment turned out to be essential for the success of the study.

The uncertainties about the positions of the sensors of the CMS detector are presented in publication V, as well as the *misalignment scenarios*, which were developed as a starting point for the alignment studies and to enable more realistic physics studies.

This thesis is organized as follows. In Chapter 2, the LHC collider is presented. Special attention is paid to its startup and expected luminosity evolution. In Chapter 3, the CMS experiment, in particular the tracker, is presented. The general alignment concept of the CMS detector is described, as well as the hardware alignment system and the reconstruction software. In Chapter 4, the HIP alignment algorithm and its applications to a simulated CMS detector and to a small test-beam setup are described. An overview of the other existing track-based alignment algorithms is given, including those being developed within the CMS collaboration. The expected alignment uncertainties of the CMS detector are discussed in Chapter 5. The corresponding software tools are presented, as well as the ready-made misalignment scenarios. Results on the impact of misalignment on track reconstruction are presented. Finally, conclusions are given in Chapter 6.

2 The LHC Collider

The LHC, illustrated in Fig. 2.1, will become the world's most energetic and largest particle accelerator with its circumference of 27 km. It is scheduled to start operation in November 2007, and it is currently being built 50–100 m underground in a tunnel of the preceding Large Electron-Positron (LEP) collider, which was dismantled at the end of 2000.

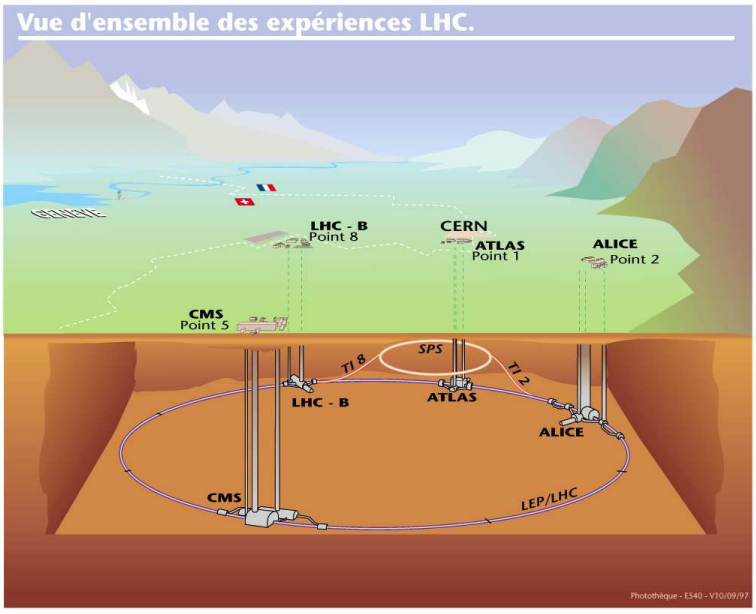

Figure 2.1: Schematic picture of the LHC collider near Geneva, Switzerland, and the positions of the experiments along it. The pre-accelerator SPS is also shown. The Jura mountains are on the right, and the Alps on the left.

In the LHC, two particle beams are accelerated in opposite directions, and made to collide in four interaction points. Physics experiments are built around these points. The ATLAS (*A Toroidal LHC ApparatuS*) [2] experiment is built at Point 1, just below the CERN main area, and CMS is built at the opposite point of the collider, together with the TOTEM experiment (*Total Cross Section, Elastic Scattering and Diffraction Dissociation*) [3].

CMS and ATLAS experiments are general-purpose detectors designed to be able to detect various particles over a wide energy range and an almost full solid angle. Both experiments focus their effort on the discovery of the Higgs boson, and therefore they both are designed to discover it over the whole range of allowed masses, which, in 1994[1], was about 80 GeV–1 TeV for the Standard Model Higgs [1]. Both experiments also have a large number of various other physics goals [5, 6].

[1]The current range of allowed masses for the Standard Model Higgs at the beginning of 2007 is 114–166 GeV, lower bound set by direct search of the LEP experiments, and upper bound by the precision measurements of electroweak observables with the top quark mass as of July 2006. Both bounds are at a 95% confidence level [4].

2.1 LHC Design Parameters

The LHC machine utilizes eight radio-frequency cavities per beam to accelerate protons up to an energy of 7 TeV, and 1232 dipole magnets to keep the particles on a circular path. The machine can also collide heavy ions, e.g. lead nuclei, with an energy of 2.76 TeV per nucleon. Beams are not continuous, but consist of groups of particles, bunches. Each full bunch contains about 10^{11} protons.

The bunch crossings take place at a rate of 40 MHz. The design luminosity of the LHC machine is $L = 10^{34}\text{cm}^{-2}\text{s}^{-1}$. Since the total proton-proton cross section is about 100 mb, approximately 1 billion proton-proton interactions take place per second at each interaction point.

Bunches are initially formed in the 26 GeV Proton Synchrotron (PS) accelerator. Particles are accelerated to an energy of 450 GeV in the Super Proton Synchrotron (SPS), and then transferred to the LHC. The separation in time between adjacent bunches is 25 ns or 7.5 m in physical length. There will be 2808 bunches per beam in each LHC ring, and, in addition, some empty gaps between them for beam injection, dumping and synchronization purposes. The luminosity lifetime of the LHC machine is foreseen to be about 15 hours for proton-proton collisions [7].

In the interaction points, the beam is squeezed to small dimensions to generate as many proton-proton collisions as possible for each collision of bunches (bunch crossing). The RMS of the beam size at the interaction point is expected to be $\sigma = 16.7\,\mu$m in the transverse plane. At the design luminosity of the LHC, each crossing of full bunches results in a mean of 20 superimposed inelastic scatterings, in which the protons break up. As a result, about 1000 charged particles emerge from the interaction point. In addition, there are typically about 15 collisions from elastic and diffractive scattering which mostly remain undetected as their collision products escape along the beam pipe.

2.2 Startup and Expected Luminosity Evolution

The operation of the LHC will start by establishing a single circulating beam with only one proton bunch, followed by several phases of operation with increasing complexity.

The first calibration runs will consist of circulating beams of 450 GeV, the injection energy from the SPS. Proton bunches of a reduced size (5–10×10^9 protons) will be used. During the calibration run, various checks will be carried out on safety systems, beam instrumentation and hardware systems. At the end of this run, two beam operations as well as the first collisions at this energy will be carried out.

A one-month pilot physics run will follow the calibration runs. At first, 43 bunches will be used with bunch intensities of approximately 10^{10} protons. Several improvements will be carried out during the pilot physics run to further increase the beam intensity. These

improvements will be moving to 156 bunches per beam, a partial squeeze of the beam, and an increase of the bunch intensity to 4×10^{10} protons per bunch. Luminosities of $2 \times 10^{31}\,\mathrm{cm}^{-2}\mathrm{s}^{-1}$ are estimated to be attainable in this phase. During a month-long pilot physics run one could collect an integrated luminosity of $10\,\mathrm{pb}^{-1}$ [7].

Commissioning of the LHC at 7 TeV energy is scheduled for the first half of 2008. The LHC operation will start with 75 ns bunch spacing, which corresponds to 936 bunches per beam. In this mode, luminosities of $10^{32}\,\mathrm{cm}^{-2}\mathrm{s}^{-1}$ will be within reach for CMS and ATLAS, and even $10^{33}\,\mathrm{cm}^{-2}\mathrm{s}^{-1}$, if experiments are ready for bunch intensities of 10^{11} protons per bunch [8].

As nominal LHC machine parameters have been achieved in the 75 ns mode, it is desirable to move quickly to a bunch spacing of 25 ns. Operation in this mode will begin with modest bunch intensities, although peak luminosities can reach $2 \times 10^{33}\,\mathrm{cm}^{-2}\mathrm{s}^{-1}$.

During the first full year of physics running, the LHC should reach a peak luminosity of $2 \times 10^{33}\mathrm{cm}^{-2}\mathrm{s}^{-1}$ (the *low luminosity* of the LHC). However, the integrated luminosity will most likely be limited by the time taken to understand the operation of the LHC. The integrated luminosity is expected to be about $5\,\mathrm{fb}^{-1}$ in the first year, but might well be much lower, as prolonged machine-development periods may be required and higher inefficiencies than foreseen may be encountered [7].

The nominal luminosity cannot be achieved during the first years of operation, since the beam dump and collimation systems are staged, which limits the beam current. The final beam dump and collimator configurations will be installed in 2010, and nominal performance with 25 ns bunches and 1.15×10^{11} protons per bunch should be attained resulting in a luminosity of $10^{34}\,\mathrm{cm}^{-2}\mathrm{s}^{-1}$.

3 The CMS Experiment

CMS collaboration is a joint effort of more than 2 000 scientists representing 160 institutes and 37 countries. The experiment consists of the physical detector itself as well as of the related electronics, hardware and software. The overall construction costs of CMS are 525 million CHF.

The CMS experiment has been optimized [1] to explore physics at the TeV energy scale, in particular to

- discover the Higgs boson,
- to look for evidence of supersymmetry and other theories beyond the Standard Model, and
- to be able to study aspects of heavy ion collisions at unprecedented energy densities.

The CMS detector is currently being constructed and installed in the underground cavern of Point 5 in the LHC tunnel. The cavern during the lowering of the second endcap disc is shown in Fig. 3.1. CMS will be closed and ready for collisions in the second half of 2007.

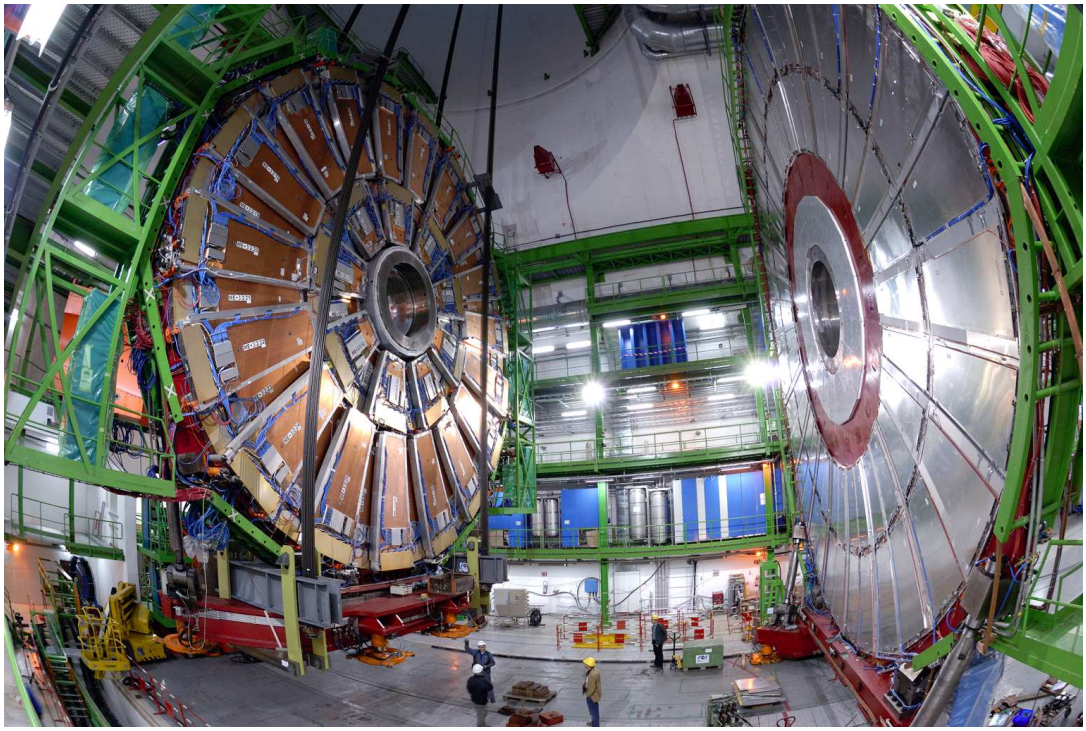

Figure 3.1: The second large endcap disc (left) was lowered into the underground experimental cavern on 12th December 2006. It took ten hours to lower the piece of 880 tonnes.

3.1 Design Criteria and Overview

CMS is designed as a compact general-purpose particle physics detector, which could be operated at the highest luminosity of the LHC. An important design criterion is the capability to measure accurately the momentum of muons from the track curvature induced by the magnetic field. Requirements of compactness of the detector and large bending power of the magnetic field have led to a choice of a very powerful superconducting solenoid magnet large enough to surround the whole calorimetric system, so that the coil does not decrease the calorimeter performance. The inner diameter of the magnet is 5.9 m and its length is 12.9 m, which makes it the world's largest solenoid magnet. It is capable of generating a 4 T magnetic field.

The design goals of CMS were defined in 1992 as [1]:

1. a very good and redundant muon system,
2. the best possible electromagnetic calorimeter consistent with 1),
3. high-quality central tracking to achieve 1) and 2), and
4. a financially affordable detector.

The CMS experiment is illustrated in Fig. 3.2. Its dimensions are 21.6 m in length and 14.6 m in diameter, while its total weight is 12 500 tonnes [9]. Most of the mass of the CMS detector is due to its solenoid magnet equipped with an iron return yoke, which is also used to support all barrel detector components [1]. The subsystems of CMS are the solenoid magnet, the hadron and electromagnetic calorimeters (HCAL and ECAL), the muon system and the tracker. The Trigger & Data Acquisition system (TriDAS) is also considered to be one subsystem.

CMS is designed to be as hermetic as possible, covering nearly the full solid angle around the interaction point. However, unavoidable blind regions exist around the beam line. The coverage of the tracker is up to $|\eta| < 2.4$[2], whereas the HCAL provides coverage of $|\eta| < 5.0$ and ECAL up to $|\eta| < 3.0$. The muon system covers the region $|\eta| < 2.4$. Good geometrical coverage is needed for reliable reconstruction of missing transverse energy and momentum from the respective conservation principles. These measurements are particularly important, since they are utilized to deduce the appearance of particles otherwise impossible to observe, such as neutrinos or other weakly or non-interacting stable particles.

CMS Tracker

The innermost part of CMS is the all-silicon tracker system. It consists of 9.6 million silicon microstrips and 66 million pixel elements [7]. It is the largest device of this type ever constructed, and many technological innovations have been necessary for its manufacturing.

[2]Pseudorapidity is an angular variable describing the direction of the particles: $\eta = -\log\tan\theta/2$, where θ is the angle between the particle and the beam direction toward the Jura mountains at Point 5. Values of pseudorapidity are illustrated in Fig. 3.5.

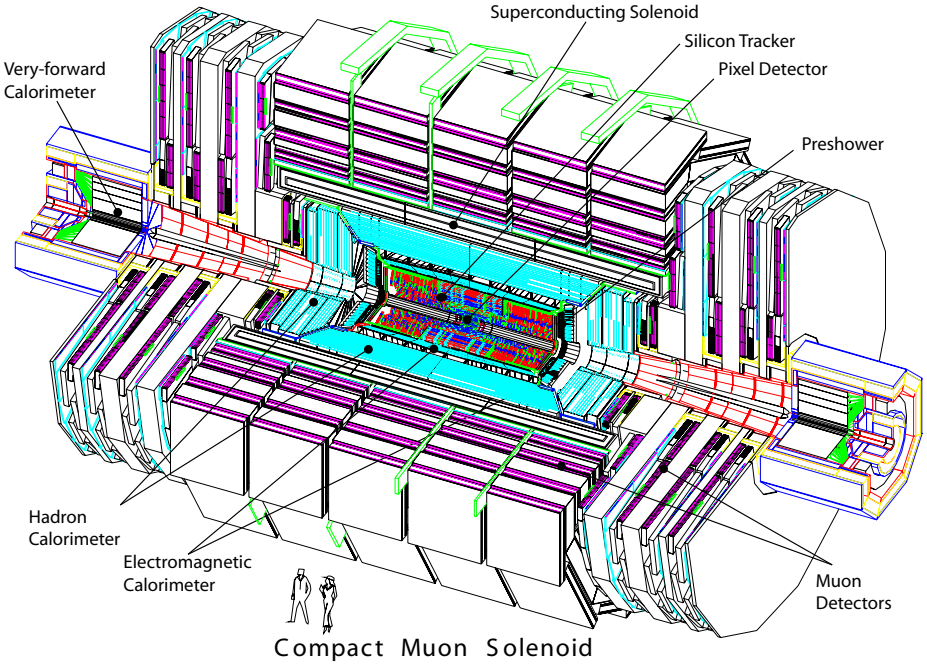

Figure 3.2: Layout of the subdetectors of the CMS detector.

The purpose of the tracker is to measure coordinates of *hits*, points where a particle has passed through a detector element, in a way that allows detailed and unambiguous reconstruction of tracks and vertices of charged particles. The tracker is used to, for instance, identify leptons and photons for isolated electromagnetic clusters, to measure momentum of energetic leptons, to tag and reconstruct b jets and B-hadrons in these jets as well as isolated τ leptons, and also to perform a precise measurement of muon momentum together with the outer muon system [9].

At the highest luminosities of the LHC, a superposition of 20-30 unrelated minimum bias events is expected at each bunch crossing, which makes correct pattern recognition challenging. Furthermore, all the material within the tracker gives rise to bremsstrahlung, which degrades both the efficiency and resolution for isolated electrons. The existence of tracker material gives rise to conversions of photons to electron-positron pairs, which leads, in particular, to loss of sensitivity in the $\mathrm{H} \rightarrow \gamma\gamma$ channel. Tracker material also gives rise to multiple scattering, which significantly degrades momentum resolution. At a transverse momentum of $p_{\mathrm{T}} = 100\,\mathrm{GeV}/c$, the material in the tracker accounts for 20-30 % of the transverse momentum resolution of muons, while, at lower momenta, the resolution is dominated by multiple scattering and reflects the amount of material traversed by the track [7]. Therefore, severe constraints are imposed on the material budget of the tracker, which is built from materials that are as light as possible.

The tracker is illustrated in Fig. 3.3. The outer radius of the CMS tracker extends to nearly 1.1 m, and its total length is approximately 5.4 m. The innermost part is the pixel

detector, which consists of the pixel barrel and of pixel endcaps. The pixel detector is surrounded by the outer part of tracker in which silicon microstrip detectors are used (the *strip tracker*). It consists of the Tracker Inner Barrel (the TIB) and Tracker Outer Barrel (the TOB), and of the two disc-like structures: Tracker Inner Discs (the TID) and Tracker Endcap (the TEC).

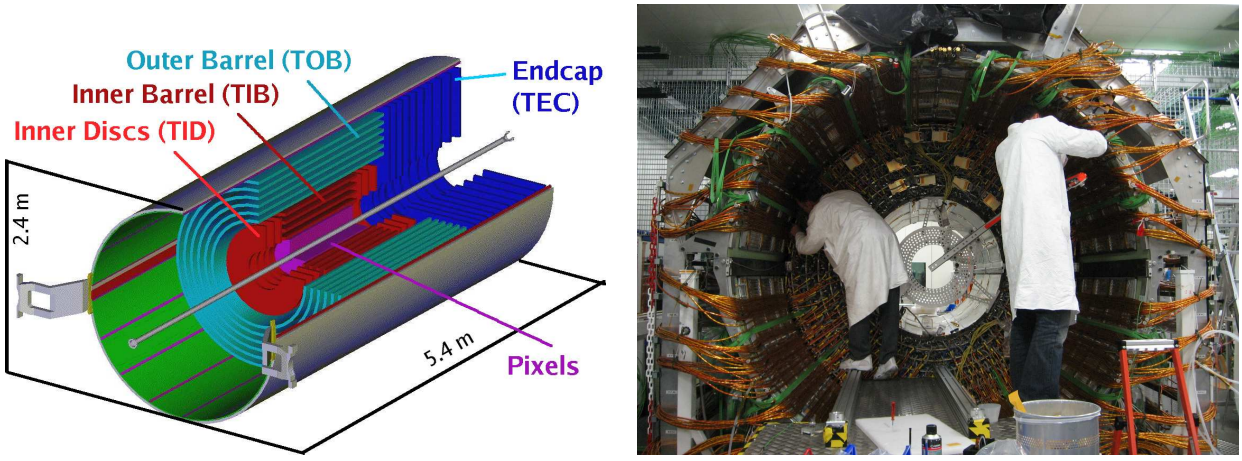

Figure 3.3: Illustration of the CMS tracker and photograph of installation of the TOB to the support tube (courtesy CMS TOB team). Total weight of the tracker is about 3000 kg, including the thermal shield and support tube.

The pixel detector is shown in Fig. 3.4. It consists of three barrel layers and two turbine-like endcap discs on each side. The barrel layers are located at a mean radii of 4.4 cm, 7.3 cm and 10.2 cm, and have a length of 53 cm. The endcap discs range from 6 to 15 cm in radius, and are placed at distances of 34.5 cm and 46.5 cm from the interaction point.

The pixel barrel layers are equipped with 768 pixel modules, which have a pixel size of $100\,\mu\text{m} \times 150\,\mu\text{m}$. Modules are arranged into half-ladders of four modules. The occupancy of the pixel detector is about 10^{-4} per pixel for each bunch crossing at the high luminosity of the LHC [7]. Resolution is improved through charge-sharing in neighbouring pixels, and through the drift angle (Lorentz angle), which is the angle by which charge-carriers moving in the electric field (generated by the bias voltage) are deflected due to the effect of a perpendicular magnetic field. In the pixel barrel modules, a drift angle of 26° is expected at the start-up of detector operation, and it is expected to decrease after irradiation, since the bias voltage will be increased to compensate for the trapping of charge carriers [7].

The pixel endcap discs consist of blades rotated by 20° to benefit also from the Lorentz effect. Without this rotation, the magnetic field would be parallel to the drift direction, and no Lorentz effect would be present. The endcap discs consist of 672 pixel modules with seven different modules in each blade [7].

Like the pixel detector, the strip tracker consists of a barrel part and endcap parts, illustrated in Fig. 3.5. The barrel part is formed from the four-layer TIB and the six-layer TOB. The two first layers in the TIB and the TOB use double-sided stereo modules consisting

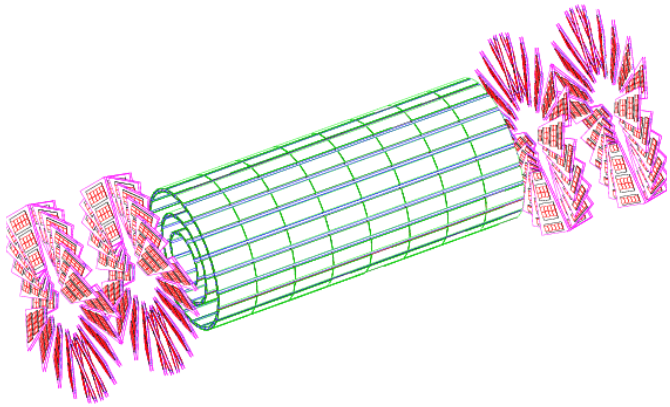

Figure 3.4: The pixel detector. Four pixel endcap discs surround the barrel part, which consists of three layers. Length of the device is about 1 m and diameter about 30 cm.

of two sensors attached back-to-back with a small stereo angle (100 mrad). These modules provide measurements in two dimensions. The strip pitch varies in the TIB from 80 to 120 μm, and in the TOB from 120 to 180 μm. The occupancy in the TIB and the TOB is of the order of 1–3 % per LHC bunch crossing at high luminosity.

The endcap strip detector is made of three inner discs (the TID) and nine outer discs (the TEC). Modules in the concentric rings 1, 2 and 5 (counted from the beam) are double sided. Strips on these modules point towards the beam line, and therefore have a variable pitch [7].

Calorimeters

The tracker system is surrounded by two calorimetric systems. Calorimeters are designed to completely stop the particle creating showers of secondary particles, and by that measure the energy deposited in the detectors. Two different calorimeters are used in CMS: the electromagnetic calorimeter (ECAL) and the hadronic calorimeter (HCAL).

The ECAL is focused on the detection of photons and electrons. It is a hermetic, homogeneous calorimeter consisting of more than 60 000 scintillating crystals made of lead tungstate ($PbWO_4$). Silicon avalanche photodiodes (APDs) are used as photodetectors in the barrel and vacuum phototriodes (VPTs) in the endcaps.

To fully benefit from the outstanding energy resolution of the ECAL, it has to be rigorously calibrated. This technically challenging operation will be carried out with laboratory tests and test-beam studies, and also with physics events such as $W \to e\nu$, in which the momentum of the electron is measured in the tracker, and can be used to calibrate the energy measurement in the ECAL. Also, to measure the energy with ECAL most accu-

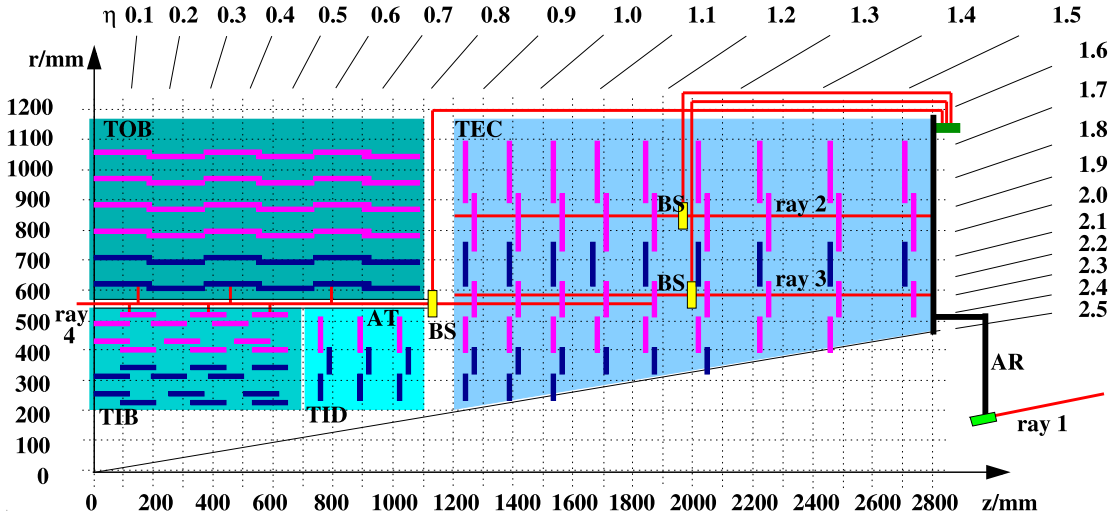

Figure 3.5: One quarter of the CMS tracker (the pixel detector is not shown). Origin is in the interaction point, and beam line coincides with the x-axis. Different parts of the tracker can be seen. Double-sided sensors are coloured in blue. The Laser Alignment System is also shown. Laser beam splitters (BS) are coloured in yellow.

rately, the tracker has to be built with materials that are as light as possible in order to minimize the possibility of interactions such as bremsstrahlung and conversions of photons to electron-positron pairs.

The HCAL is designed to detect hadrons. It consists of absorbers made of brass (for mechanical strength, some stainless steel plates are also used), and of an active material, for which plastic scintillator tiles are used [7].

Muon System

The outermost layer of CMS consists of the muon detectors designed to identify and measure high-energy muons. Muons are not stopped by the hadron calorimeter, and, ideally, they should be the only particles detected in the muon system. The muon chambers consist of aluminium drift tubes (DT) in the barrel region and cathode strip chambers (CSCs) in the endcap region, complemented by resistive plate chambers (RPCs), which provide a redundant fast trigger signal.

Muons originating from the primary vertex are measured three times. The first measurement takes place in the inner tracker, then the second after the coil, and the third in the return flux of the magnetic field. Momentum can be determined either with the muon system alone (from the bending angle at the exit of the 4 T coil), or with the curvature measured by the tracker, or with both. Momentum resolution is dominated by the silicon

tracker, but, for muons with momentum higher than a few hundred GeV/c, this resolution can be further improved by combining measurements of the inner tracker and muon detector. In this case, when multiple scattering and energy loss can be neglected, the muon trajectory beyond the return yoke can be extrapolated back to the beam line, which can be used to improve the muon momentum resolution [7].

Track Reconstruction

Track reconstruction in CMS proceeds through the following five stages [7]:

- hit reconstruction, in which position and uncertainty of hits are deduced from signals of the corresponding detector elements,
- seed generation, in which trajectory seeds are generated from pairs of hits in the pixel detector,
- pattern recognition or trajectory building, in which the combinatorial Kalman Filter [10] is propagated from layer to layer, adding trajectory candidates for each compatible hit,
- trajectory cleaning or ambiguity resolution, in which mutually exclusive track candidates are resolved, and
- final track fit.

As a result of track reconstruction, each track is described with five parameters, which define its point of closest approach to the beam, the direction of the momentum vector of the track, and the transverse momentum. Particle identification of muons, electrons and photons is based on combining tracking and calorimetry information (for instance, photons are detected only in the electromagnetic calorimeter). Identification of short-lived heavy flavor particles (b- or τ-tagging) utilizes several methods, for instance, the evaluation of the statistical significance of the shortest distance between the track and the interaction point (the *impact parameter*).

In order to select only interesting tracks from the large background, several selection criteria need to be used. For instance, to reconstruct events with $Z^0 \to \mu^+\mu^-$, one would require two tracks with a muon detection in the muon chambers and an invariant mass compatible with m_{Z^0}.

3.2 General Alignment Concept of the CMS Detector

Individual sensors of CMS tracking devices — the pixel detector, the strip tracker and the muon chambers (DTs and CSCs) — have an excellent intrinsic spatial resolution. For the approximately 20 000 silicon sensors of the tracker, it is in the range of 10–50 μm [9], and for the about 1 400 muon chambers and drift tubes, in the range of 75–100 μm [11].

Resolutions of individual silicon sensors lead to a single-point resolution of 23–34 μm in the r-ϕ direction[3] and 230 μm in z in the TIB. In the first two layers of the TOB the resolution is 35–52 μm in the r-ϕ direction and 530 μm in z. In the pixel detector, the spatial resolution is measured to be about 10 μm for the r-ϕ measurement and about 20 μm for the z measurement [7]. Measurements in the r-ϕ direction are used to define the curvature and the momentum in the r-ϕ plane, and therefore they need to be more accurate than the measurement in the z direction.

The overall tracking performance is, however, degraded by *alignment uncertainties*, the imperfect knowledge of the positions and orientations of the individual sensors. These uncertainties are in the range of 100–500 μm after the installation of CMS [7], and they are among the largest potential sources of tracking uncertainties. Other sources of tracking uncertainties are, for instance, imperfect knowledge of the magnetic field and drift angle in the silicon sensors and imperfect material description. Specific *alignment* procedures are needed to decrease alignment uncertainties down to a level comparable to, or preferably better than, the intrinsic sensor resolution. Similar requirements are imposed on the muon system.

The required level of alignment precision can only be achieved with a track-based alignment procedure. However, other methods are also needed as a starting point for track-based alignment algorithms, since pattern recognition and reconstruction require an accuracy better than the placement precision of the assembly. In addition, continuous alignment is also needed to monitor and correct time-dependent effects, which can appear, for instance, because of changes of humidity and gas evaporation from the carbon fibre supports. One important source of misalignment for the muon system is the deformation caused by the magnetic field: for instance, the centre of each endcap disc is estimated to deflect towards the interaction region by approximately 14 mm when the magnet is turned on [11]. This behaviour has also been measured and confirmed in the magnet tests carried out in summer, 2006.

The general alignment strategy of CMS therefore utilizes a three-step approach:

1. measurements of mounting precision during assembly of tracking devices, with, for example, photogrammetry and sensor position survey measurements,
2. measurements of relative positions of subdetectors with lasers, transparent sensors, light sources and TV-cameras, and
3. track-based alignment.

The two first approaches are used to reach a level of about 100 μm for the alignment uncertainties at the very beginning of data taking. This level is needed to start efficient pattern recognition, which allows the use of track-based alignment to further improve the alignment of individual sensors.

[3]The coordinate system in CMS is such that the origin is in the nominal collision point, y axis is vertically upward, x is towards the centre of the LHC ring, and thus z is along the beam line pointing towards the Jura mountains. The azimuthal angle ϕ is measured from the x-axis in the x-y plane. The polar angle θ is measured from the z-axis.

The general alignment strategy proceeds with track-based alignment as follows: first the tracker will be aligned standalone, beginning with the pixel detector[4], then covering the strip detector. Then the muon system will be aligned with the tracker, and finally the calorimeter modules will be adjusted to the aligned tracking devices. Therefore, the first simulated alignment studies, as in publications II and IV, concentrate on the alignment of the pixel detector.

3.3 Survey Measurements and Hardware Alignment

During the assembly of the CMS tracker, positions and orientations of tracker detector components are measured and stored in databases. Measurements are carried out with, for example, coordinate measurement machines or photogrammetry. Some measurements are carried out comprehensively for all manufactured parts, and some measurements only for a sample. If measurements are carried out for all silicon detectors, they are saved in a database, and used as corrections to the ideal tracker geometry. If only a sample is measured, the standard deviation of the measurements can be used as an estimate of the corresponding mounting uncertainty, and this error can be taken into account in the initial track reconstruction.

An example of survey measurements is the quality control measurements carried out for the TOB rods (support structures). These measurements were carried out for all 753 manufactured rods in Helsinki. Positions of the support elements, which were used to position the actual modules, were measured and compared to the nominal measures. The distribution of alignment corrections for all modules can be seen in publication IV.

The initial installation uncertainties of CMS subdetectors are improved with the hardware alignment system. It consists of independent systems for the tracker and the muon chambers and of a link system connecting these together. The tracker is equipped with a Laser Alignment System (LAS), which uses infrared laser beams to monitor the positions of selected detector modules. The muon alignment system (MA) consists of optical devices, which are used to align the muon barrel and the endcaps. The link system relates the muon and the tracker alignment systems and allows a simultaneous monitoring of these devices.

The hardware alignment is especially important for the muon detectors. Goals of the optical alignment for the muon system are 1) to track large displacements due to the magnetic forces affecting the return yoke, and 2) to provide long-term supervision of the detector positions and of the changes due to thermal effects. Muon detectors are mounted on the iron rings and discs acting as a magnetic flux return yoke, and therefore they are subject to displacements ranging from a few mm to 1–2 cm when the magnetic field is activated [12].

[4]It is currently foreseen that the pixel detector will be installed in CMS during the shutdown following the one-month LHC pilot physics run, and that the strip detector will have to be aligned as standalone at that time. The integrated luminosity of this run will probably be too small to fully align the strip detector, and thus alignment after the pilot physics run will be carried out as described above.

The thermal expansion of the chambers and their iron supports are expected to be in the submillimeter range [11]. These correlated displacements can be detected and corrected for the most part with the hardware alignment system.

The MA consists of three r-z alignment planes. LEDs, CCDs and laser beams are used with precise distance and angle-measuring devices. Each of the 250 drift tube chambers in the barrel is monitored, while only 23 out of the 540 chambers in the four endcap stations are directly monitored. Muon alignment can be carried out several times per hour.

The muon chambers need to be aligned with the hardware alignment system with respect to each other and with respect to the tracker, with an accuracy of 100–500 μm [7]. This ensures the optimal performance over the entire momentum range up to 1 TeV/c.

In the tracker, the LAS can monitor most of the composite structures, but the innermost pixel detector, as well the TID (see Fig. 3.5), are out of its reach. The LAS system has two goals: 1) to provide the initial alignment at the level of 100 μm to ensure tracking and reconstruction, and 2) to monitor the larger structures of the tracker on a continuous basis at the level of 10 μm. The LAS is foreseen to operate both in dedicated runs and during physics data taking.

The LAS, illustrated in Fig. 3.5, consists of 16 laser beams parallel to the LHC beam and of eight beams perpendicular to it. The 16 beams are distributed equally in ϕ in the endcaps. These beams cross all nine discs, and allow the internal alignment of the TEC. The other eight beams are used to align the TIB and the TOB, and both TECs, with respect to each other. A link to the muon system is established by another 12 beams.

Positioning uncertainties after the survey measurement and application of the hardware alignment systems is further discussed in Chapter 5, where the implementation of *misalignment scenarios* is presented.

4 Track-Based Alignment

Track-based alignment (TBA) carried out with software is the most accurate method for alignment of large tracking detectors. It has been used and reported by several particle physics experiments. These methods are, however, not directly applicable to CMS, because the large number of degrees of freedom involved makes them computationally impossible.

The principle of track-based alignment is illustrated in Fig. 4.1. A hit signifies coordinates of a particle measured by the sensor itself. The impact point is the crossing of a reconstructed track on the sensors. Fit residuals are the differences between a hit and the associated reconstructed track. With fit residuals of a large number of tracks, knowledge of the position of the sensor can be corrected to correspond to its real position. Corrections can be calculated for all six alignment parameters (three translations and three rotations). Larger and more complex composite objects can be aligned in a similar way.

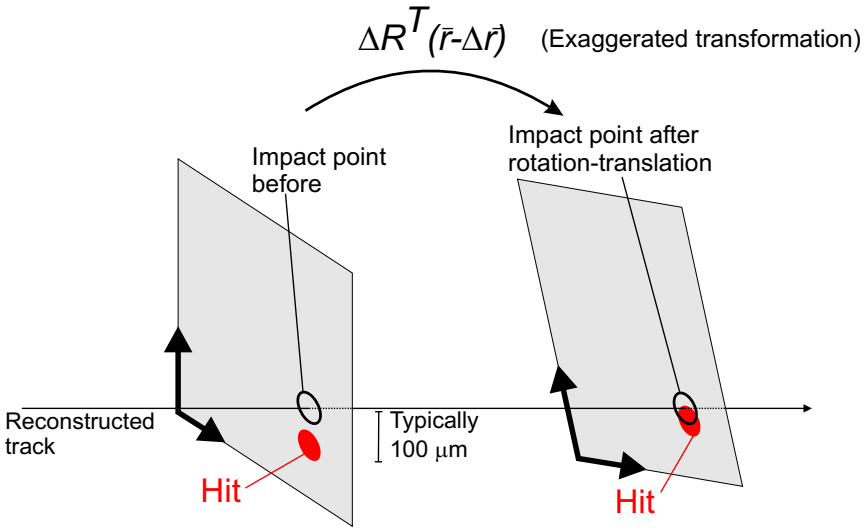

Figure 4.1: Principle of alignment. ΔR and $\Delta\bar{r}$ signify the alignment corrections, rotation and translation, to the position of the detector unit $\bar{r}$. Transformation changes the local (detector) coordinates of the impact point.

4.1 Track-Based Alignment in Particle Physics Experiments

Methods of track-based alignment have been used in several, presumably in a majority of, High Energy Physics (HEP) experiments. However, only a few of them have been reported in publications. A review of their mathematical principles can be found in [13].

In the ALEPH experiment, alignment was carried out for the 144 wafers of the silicon vertex detector (VDET). Computing time was already an issue for this problem of 864 alignment parameters, and therefore alignment was carried out wafer by wafer in an iterative way. A vertex constraint was used, and with 20 000 $Z^0 \to q\bar{q}$ events and 4 000 $Z^0 \to \mu^+\mu^-$ events[5], an accuracy of a few μm was achieved, which was clearly below the intrinsic resolution of 10 μm of the detector elements [14, 15].

In the DELPHI experiment, $Z^0 \to \mu^+\mu^-$ events and cosmic muons were used for the global alignment between subdetectors Vertex Detector (VD), Outer Detector (OD) and Time Projection Chamber (TPC) [16]. In the final internal alignment of the barrel part of the Silicon Tracker with LEP2 data, predefined functions were fitted to the residual distributions. These functions corresponded to the six degrees of freedom of individual detector staves (each holding four or eight detector plaquettes) and also to certain parameterized internal deformations, to the radial bending, for instance. The iterative process utilized $Z^0 \to \mu^+\mu^-$ events, together with information from overlaps of detectors and hadronic tracks passing through all three layers. The achieved average single-layer resolution in the r-ϕ direction was better than 8 μm [17].

Track-based alignment was in regular use in the LEP2 experiments. At the beginning of each yearly LEP run, a short run of 1–2 pb^{-1} was carried out at $\sqrt{s} \approx m_{Z^0}$, which could be used for alignment purposes [18].

A computationally challenging approach was chosen in the track-based alignment of the SLD experiment, in which 96 CCD elements were aligned. The algorithm involved finding a pseudoinverse for a matrix of size 2108×578 through singular value decomposition [19, 20].

In the BaBar experiment, which is currently taking data, the alignment program has played a crucial role for the performance of the silicon-vertex tracker (SVT) for the precise measurement of the decay position of B mesons. Alignment in BaBar consists of internal alignment of the SVT and the global alignment between the SVT and the drift chamber. Internal alignment of the SVT is carried out with standalone tracking every one to two months. A χ^2-minimization procedure is applied to di-muon events and cosmic muons, and information from overlaps of detectors is taken into account. In the global alignment, the SVT is considered as a rigid body, and alignment between the SVT and the drift chamber is computed. Because of the daily movements of the SVT, global alignment is carried out continually with events collected during the last hour [21].

The H1 and ZEUS experiments at the DESY accelerator centre have applied the Millepede method to their alignment [22, 23]. Tracks from the electron-proton interactions as well as cosmic muons have been utilized. An iterative method based on χ^2-minimization has also been recently used in the alignment of the ZEUS micro-vertex detector [24]. The CDF experiment in Fermilab has reported alignment based on fits to the residual functions in Ref. [25], as well as about a feasibility study for the Millepede method with 352×3 alignment parameters in Ref. [26].

[5] The Z^0 sample was statistically limited during the LEP2 runs.

In the DØ experiment, which is also currently taking data, about 850 sensitive elements of the Silicon Microstrip Detector (SMT) were aligned in Ref. [27]. Each detector was aligned individually with tracks fitted to all other detectors, and corrected positions served as input geometry for the next iterative step. The obtained precision was close to the design value (residuals of 20 μm compared to simulated residuals of 16 μm).

In ATLAS, three methods are envisaged for the track-based alignment of the Inner Detector (ID). A global fit method [28, 29], similar to the Millepede algorithm developed for CMS [30], is used to align all 5 800 silicon modules of the pixel and silicon strip detector, as well as the track parameters, simultaneously. This approach involves solving a matrix equation with a matrix of a size of $35\,000^2$. A large computer cluster with 64-bit CPU architecture has been suggested for this purpose [31]. A method with local fit, in which detectors are aligned individually, is also proposed, as well as a robust method, which only takes into account mean residuals, mean overlap residuals and alignment of neighbouring modules. This robust method can be used in practice to align 2–3 degrees of freedom.

Track-based alignment is also beneficial in small-scale setups. Publication VII presents the results of a test beam experiment performed with the Silicon Beam Telescope (SiBT) [32] detector. The telescope is situated at CERN and operated by Helsinki Institute of Physics. It is illustrated in Fig. 4.2. It consists of 6–8 microstrip detectors, and is used to provide reference measurements of tracks needed in detector development. In publication VII, it was used to characterize a heavily irradiated microstrip detector made of magnetic n-type Czochralski silicon. Rigorous alignment of the two reference detectors and the Czochralski silicon detector was required to distinguish the signal hits from the fake hits caused by the high noise level of the irradiated detector.

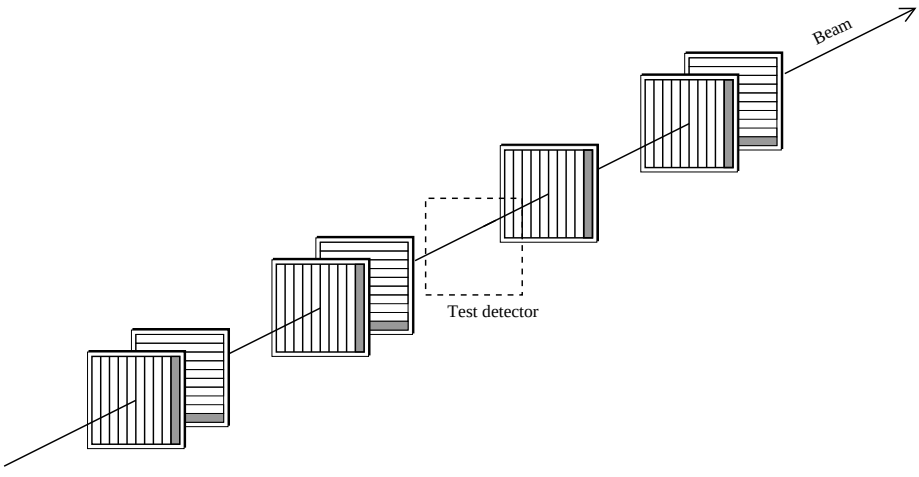

Figure 4.2: Schematic diagram of Silicon Beam Telescope. Length of the device is about 0.5 m, and detectors have an active area of $5.6 \times 5.6\,\mathrm{cm}^2$.

4.2 Track-Based Alignment Algorithms and Data Samples in CMS

In CMS, track-based alignment is important, especially for the pixel detector and the TID, since they are out of reach of the hardware alignment system, and their alignment relies completely on the TBA. For track-based alignment, a good algorithm is, of course, necessary, but also proper data is essential. If only homogeneous data is used (for instance, tracks coming solely from the interaction point), detector units are not constrained sufficiently, and the algorithm may give incorrect results, degrading physics results.

Track-Based Alignment Algorithms

Even though careful alignment procedures have been carried out in many existing particle physics experiments, new approaches are needed for the CMS detector. The major challenge in CMS is the enormous number of degrees of freedom involved. For the tracker alone, there are 20 000 individual sensors, so to fully align the tracker, about 10^5 alignment parameters have to be solved. The straightforward way of solving the alignment problem involves an inversion of the fit matrix of size $10^5 \times 10^5$. Inversion of a matrix of this size is practically impossible (although this approach seems still to be possible for the ATLAS Inner Detector, with its 5 800 silicon modules [31]), and therefore different approaches are used, either to solve the matrix equation by other means, or to avoid these equations. For the CMS muon system, the straightforward alignment problem is still solvable — there are 790 individual chambers and about 5 000 alignment parameters.

Of course, a partial alignment could be carried out for the CMS tracker by, for instance, considering only barrel layers or larger support structures, but since the mounting uncertainties of individual sensors is larger than their intrinsic resolution (see Chapter 5.1), alignment of individual sensors will eventually be necessary. Alignment could also be carried out for separate parts of the tracker (for instance, only for the pixel detector or TOB), but in that case, one would have to make sure that misalignments of other tracker parts do not bias the results. This could be achieved by, for instance, refitting the tracks. These two simplified approaches can be very useful, especially when only a small amount of data is available, but to make the best possible alignment with all available measurements, a full alignment for individual sensors is needed.

Three alignment algorithms are implemented and studied within CMS — the HIP algorithm, the Kalman filter algorithm [33], and the Millepede algorithm [30]. The algorithms use a common software interface, which provides the necessary derivatives and residual information. The first results of their use can be found in Ref. [7]. A variant of the Millepede algorithm is currently applied to the muon system, whereas the feasibility of all algorithms is studied for the tracker.

Developing several algorithms serves to crosscheck their results. Their feasibility in different tasks can also be compared. Publication IV illustrates this possibility with the first

comparison between the results of two algorithms (the HIP and Millepede algorithms), as well as manually obtained results for the alignment of a test-beam setup.

The HIP method is a straightforward and computationally light way to solve the alignment problem. The method consists of iterative steps of alignment and refitting the tracks. All desired sensor modules are aligned independently, and correlations between modules are included implicitly via correlations between residuals in the track fit. The advantage of this algorithm is its very low computational requirement: only a 6x6 matrix inversion is required for each alignable object.

The Kalman Filter algorithm is a method for global alignment based on the Kalman Filter [33, 34]. Its fundamental idea is to update alignment parameters after each track. Correlations of all sensor modules are stored to a correlation metrics list, so that an update of the alignment parameters can also be carried out for those detector units with significant correlations with units crossed by the track. This approach avoids inversion of large matrices, but requires continuous updating of the correlation list

The Millepede approach has been used in, for example, CDF [26] and other experiments. It is a non-iterative linear least squares algorithm, which fits both the track parameters and alignment parameters simultaneously and uses all available information for solving the alignment problem. Millepede solves the full correlation matrix of size $6N \times 6N$, where N is the number of sensors to be aligned, by inversion (Millepede1 [22]). Matrix inversion, however, requires CPU time proportional to the third power of the size of the matrix, and therefore a computationally easier version envisaged for CMS that solves the matrix equation by an iterative way has been developed (Millepede2 [30]). A variant of Millepede1 has been utilized for muon alignment in CMS. This version also takes into account the direction of the track measured by the individual muon chambers.

Data Samples for Track-Based Alignment

Properties of available tracks have significant importance for the success of the alignment algorithm. In residual-based methods, alignment of all six degrees of freedom of an individual sensor with a one-dimensional measure can lead to more than one solution (it can be a geometrically underconstrained system having a non-zero dimensional solution space). This can be avoided by using tracks, which cross the sensor at various angles and also cover the full active area of the sensor.

From the point of view of the whole detector, *global* χ^2*-invariant distortions* need to be considered. These are deformations under which tracks still remain helices, but with different properties. These deformations cannot be measured or corrected by track-based alignment, especially if a homogeneous track sample (tracks which do not relate all parts of detector together) and no additional constraints are used. Such deformations can take place in the detector and remain uncorrected, and, also, the TBA algorithm may generate such deformations during the alignment process. They consist of small changes in individual sensors, which add up coherently in the detector. Examples of global distortions include barrel

rotation according to $\Delta\phi \sim ar^2 + br + c$, translation of barrels in x-y plane, illustrated in Fig. 4.3, as well as radial expansion of the whole detector, twist of barrel parts, etc. They can introduce a significant bias to physics results.

To control global distortions, a heterogeneous sample of tracks covering and relating as many parts of the detector as possible is needed. Also, additional constraints like mass constraints, E/p constraints obtained from calorimeters, use of overlapping hits from adjacent detector modules and mechanical properties of the detector can be beneficial. For instance, the rotation of Fig. 4.3 can be observed and corrected by charge-symmetric p_{T} distributions (for instance, $Z^0 \to \mu^+\mu^-$ events), since the bias of p_{T} is opposite for positively and negatively charged tracks. For the x-y translation, the dependence of E/p from ϕ could be utilized. Global distortions and how to control them will be an important topic when the detailed alignment strategy for CMS is planned.

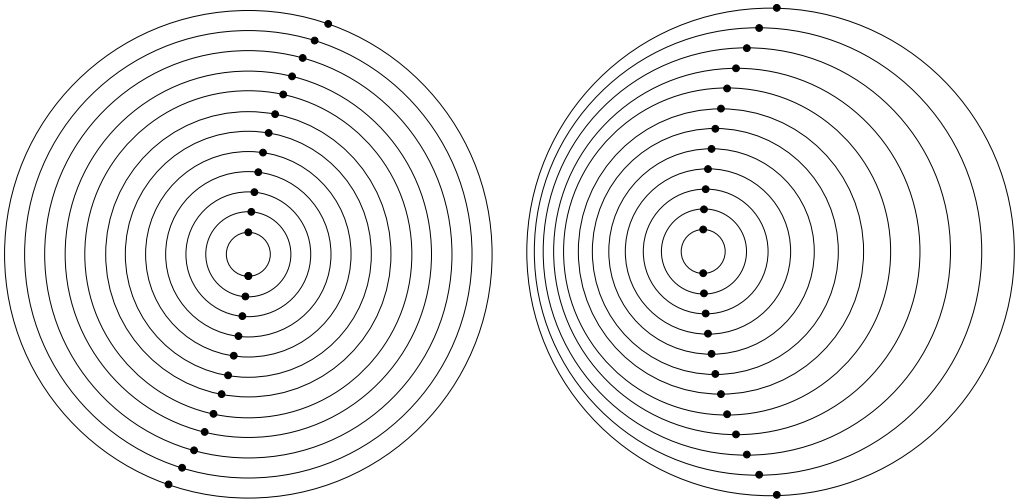

Figure 4.3: Examples of χ^2-invariant global distortions, under which tracks still remain as helices. Left: barrel rotation according to $\Delta\phi \sim ar^2 + br + c$; Right: barrel translation in xy-plane.

The most fundamental global distortion of a particle detector is its global translation or rotation in space; this requires special attention. This distortion does not affect physics results, but can lead to instability of the alignment. This distortion can be avoided by using external measurements of, for instance, modules surveyed by hardware alignment, or by constraining the average global displacement and rotation to be zero.

The $Z^0 \to \mu^+\mu^-$ and $W^\pm \to \mu^\pm\nu$ data samples are the most useful single kind of events for TBA, since their rate is relatively high, muon momentum is measured accurately, and muons also connect the tracker with the muon system. They, however, have all a similar homogeneous topology: they arrive from the interaction point. For alignment, additional tracks with different topology would be needed.

At low luminosity of $L = 10^{33}\,\mathrm{cm}^{-2}\mathrm{s}^{-1}$, about 20 000 Z^0 and 10^5 $W^\pm$ events are selected per day in CMS by the High Level Trigger (HLT) [35]. It is estimated that 1–2 million

tracks are enough for full TBA of the tracker [7]. Therefore, 1–2 weeks of data taking at low LHC luminosity would be enough to fully align the tracker [7].For the muon system, a few days of running time would be sufficient [7].

To complement the alignment information of tracks originating from the vertex region, other event samples like cosmic muons, as well as beam gas and beam halo muons, are useful. Tracks of cosmic muons are near to vertical and their rate is independent of the LHC operation, whereas beam gas and beam halo tracks are machine-induced events almost parallel to the beam line (they are present already in single-beam operation).

Cosmic muons are foreseen to be used in the alignment of both the tracker and the muon system [11]. Since the CMS cavern is 100 m below ground, most cosmic muons enter the cavern through the maintenance shaft. They can, however, cover the whole CMS [36]. Vertical cosmic tracks are especially useful for barrel region alignment. It is estimated in Ref. [36] that, each hour, 700 high-energy cosmic muons cross the entire barrel part of the tracker (the TOB, the TIB and the pixel barrel). Dedicated cosmic runs are foreseen between the LHC machine operations.

Beam gas events have an event topology similar to collision events, but they have a softer p_{T} spectrum ($p_{\mathrm{T}} < 2\,\mathrm{GeV}/c$) with a centre-of-mass energy $\mathrm{E_{cm}} = 115\,\mathrm{GeV}$ for 7 TeV proton beams. However, the soft p_{T} spectrum makes them hard to be triggered, and also limits their use to the inner part of CMS (i.e. to the tracker).

Beam halo muons are machine-induced secondary particles, which cross CMS almost horizontally. They would be very useful for the endcap region as they connect the two ends of the apparatus. However, a specific trigger is needed. Muon chambers could be used for this purpose, but they do not cover the tracker region. One possibility would be to use the TOTEM [3] T1 telescopes for triggering when they are operated at luminosities lower than $L = 10^{32}\,\mathrm{cm^{-2}s^{-1}}$.

The possibility of also using tracks from minimum bias (MB) events is studied. Especially during the first data-taking period, with low LHC luminosity and smaller collision energy, these events can provide a sufficient amount of tracks for alignment. Unlike in, for example, $Z^0 \to \mu^+\mu^-$ events, more than two useful tracks in MB events may emerge from the primary vertex, which can be utilized as a constraint. Tracks in MB events have low p_{T} value, typically smaller than $5\,\mathrm{GeV}/c$, leading to larger hit residuals due to multiple scattering. The larger spread in the hit residuals can be compensated by considering a larger amount of MB events to achieve sufficient statistical significance.

4.3 Hits and Impact Points Algorithm

The HIP method presented in publications II and III, and used in publications IV and VI, is a straightforward alignment algorithm, originally developed for the SiBT [37, 38]. The method is computationally light: for each sensor, only a 6x6 matrix is inverted. The

method can be applied for either individual sensors or composite objects consisting of a number of individual sensors. In the latter case, the composite object is aligned as a rigid body, and the relative positions of individual sensors within the object are not changed. These approaches are explained in detail in publications II and III.

Composite objects can correspond to the physical support structure to which individual sensors are attached to. For instance, in the TOB, individual sensors are attached to rods, which are further attached to barrel-like structures, which then form the entire TOB subdetector. Alignment can be carried out for these different levels of hierarchy. These are illustrated in Fig. 4.4 as they are implemented in the CMS reconstruction software ORCA [39] (Object-oriented Reconstruction for CMS Analysis). Alignment of a composite object is justified by the fact that the positioning uncertainties of the composite objects can be much larger than the intrinsic sensor resolution, either as a result of installation uncertainties (see Chapter 5) or as a result of time-dependent distortion of the composite object, which does not affect the relative positions of individual sensors. Also, especially in the early operation of CMS, a small amount of tracks might be enough to align a composite object, but not yet individual sensors. Alignment of composite structures might also turn out to be very beneficial if support structures are affected by time-dependent effects that require continuous monitoring and frequent alignment.

After the alignment corrections have been applied, the tracks in the sample need to be refitted to correspond to the corrected hit positions. If large corrections are needed, it may be necessary to also repeat the pattern recognition for the tracks. Refitting tracks implicitly takes into account the correlations between residuals of different modules. Hence the HIP method consists of an iterative sequence of steps of calculation of alignment corrections and track refitting.

Residual χ^2 function

The HIP method can be used to align all six alignment parameters or their subset. The alignment parameters are the three translations in local coordinates, and the three right-handed rotations around these axes. Corrections to alignment parameters are denoted as $\Delta u, \Delta v$, Δw, $\Delta\alpha, \Delta\beta$, and $\Delta\gamma$, respectively.

The goal of the HIP method is to find for each alignable object those alignment parameters that minimize its least squares (χ^2) function of hit residuals. This function describes the quality of alignment of one individual module with respect to all tracks traversing it. It does not describe the quality of the track fit. The χ^2 function is:

$$\chi^2 = \sum_j \epsilon_j^T \mathbf{V}_j^{-1} \epsilon_j, \tag{4.1}$$

where ϵ_j is the residual vector and $\mathbf{V}$ is its covariance matrix; the subscript denotes the hit j on the alignable object. The residual vector ϵ_j is:

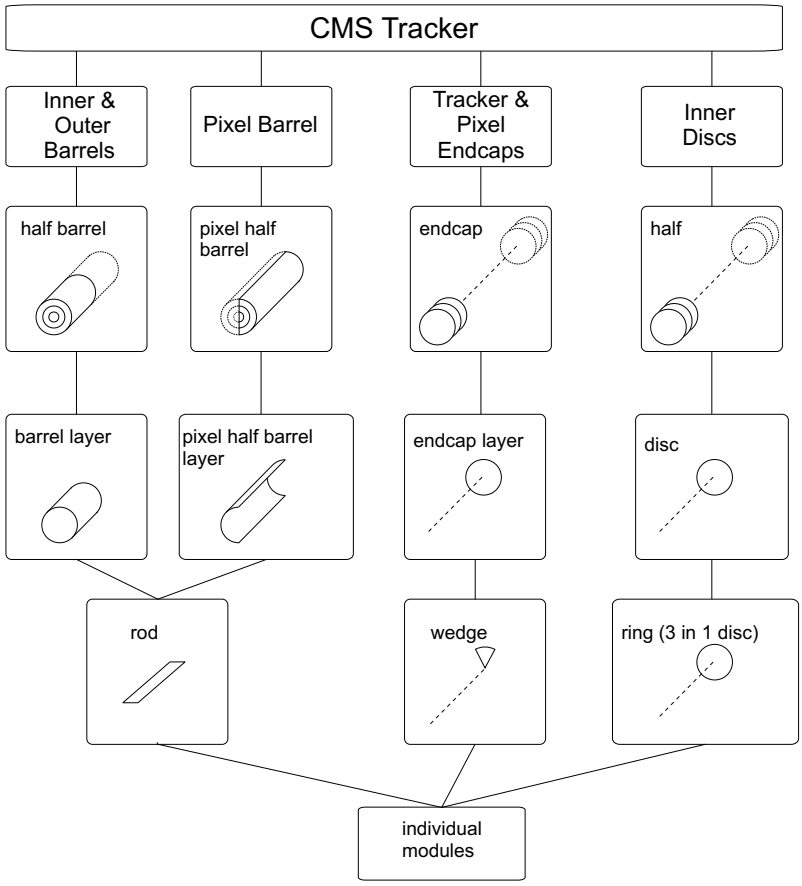

Figure 4.4: Illustration of the hierarchical structure of the CMS tracker as implemented in the reconstruction software ORCA [39].

$$\epsilon_j = \begin{pmatrix} \epsilon_{u,j} \\ \epsilon_{v,j} \end{pmatrix} = \begin{pmatrix} u_{x,j} - u_{m,j} \\ v_{x,j} - v_{m,j} \end{pmatrix}, \tag{4.2}$$

where $u_{x,j}$ and $v_{x,j}$ represent the coordinates obtained from the reconstructed track (the *impact point* coordinates), and $u_{m,j}$ and $v_{m,j}$ are the measured coordinates, all expressed in the local coordinate system. For a strip detector measuring only one coordinate ϵ_j reduces to a scalar.

The covariance matrix $\mathbf{V}_j$ of the residual vector ϵ depends on error estimates of the impact point and the measured hit. Diagonal elements of the covariance matrix are $\sigma_i^2 = \sigma_{i,x}^2 + \sigma_{i,m}^2 - 2\sigma_{i,xm}$, where i is either u or v, and the two first terms are impact point and hit resolutions, respectively[6]. The last term, their covariance, is zero if the detector is not taken into account in the track fit, giving $\sigma_i^2 = \sigma_{i,m}^2 + \sigma_{i,x}^2$. This is, however, usually not

[6]The offdiagonal elements are $\sigma_{uv} = \sigma_{uv,x} + \sigma_{uv,m} - \mathrm{cov}(u_x, v_m) - \mathrm{cov}(u_m, v_x)$.

the case, and $\sigma_{i,xm}$ has a positive value smaller than $\sigma_{i,m}^2$. In this case, the covariance can be calculated from the track fit formalism, giving $\sigma_{i,xm} = \sigma_{i,x}^2$, leading to smaller $\sigma_i^2 = \sigma_{i,m}^2 - \sigma_{i,x}^2$.

To determine the effect of alignment corrections to the residuals and to the χ^2, directions of particle trajectories need to be modelled in the vicinity of the impact point. Trajectories have the shape of a helix, but they are approximated as straight lines, which is a valid approximation in the range of alignment corrections. Also, the errors of the measurements can be regarded as constant within this range.

In practice, and especially at the beginning of the alignment process, the residual distributions may be very irregular and have several peaks due to misalignments of all sensors. In addition, a certain fraction of hits may be outliers, resulting, for example, from noise, overlapping tracks or nearby secondary particles. To avoid these practical problems and make the algorithm more robust, a quality cut can often be performed to reject outliers from the residual distribution. Also, the elements of the covariance matrix can be overestimated by assuming $\sigma_i^2 = \sigma_{i,m}^2 + \sigma_{i,x}^2$. In addition, the uncertainty due to misalignment should be taken into account in $\sigma_{i,m}^2$, for instance, by utilizing the *Alignment Position Error* approach described in Chapter 5.3. Overestimation of σ_i^2 can, however, in some circumstances lead to a slower convergence of the algorithm.

A large number of different algorithms exist for minimizing nonlinear equations such as Eq. 4.1. We have utilized the iterative method of *linear iteration* [40]. In this method, $u_{x,j}$ and $v_{x,j}$ are linearized with respect to the alignment corrections, and their second-order differentials are neglected. This is a good approximation, since the angular corrections, which give rise to the nonlinearities of the residuals, are close to zero (typically smaller than a milliradian).

Calculation of the Alignment Parameters

The alignment corrections $\mathbf{p} = (\Delta u, \Delta v, \Delta w, \Delta\alpha, \Delta\beta, \Delta\gamma)^T$ minimizing Eq. 4.1 are solved iteratively. The initial estimate is the null correction vector $\mathbf{p}_0 = \mathbf{0}$, and the iteration step is:

$$\mathbf{p}_{k+1} = \mathbf{p}_k + \left[\sum_j \mathbf{J}_j^{\mathrm{T}} \mathbf{V}_j^{-1} \mathbf{J}_j\right]^{-1} \left[\sum_j \mathbf{J}_j^{\mathrm{T}} \mathbf{V}_j^{-1} \epsilon_j\right], \tag{4.3}$$

where $\mathbf{J}_j$ is a Jacobian derivative matrix derived from the residuals. $\mathbf{J}_j$ and ϵ_j depend on the value of $\mathbf{p}_k$, and need to be recalculated for $\mathbf{p}_{k+1}$. Calculation of $\mathbf{J}_j$ is explained in the next section.

Iterations of Eq. 4.3 are performed until the χ^2 function of Eq. 4.1 converges. The convergence is reached when the change of the χ^2 function is smaller than a pre-defined value,

when, for instance, $\chi^2(\mathbf{p}_k) - \chi^2(\mathbf{p}_{k-1}) < 1.0$. Typically only a few iterations are needed for convergence.

When alignment corrections are solved for all alignable objects, their alignment parameters and coordinates are changed accordingly, and the track sample is refitted. Steps of alignment and refitting are continued until no statistically significant improvement is obtained for the alignment.

Jacobian of Individual Sensors

The Jacobian of Eq. 4.3 is a 2×6 matrix:

$$\mathbf{J}_j = \nabla_{\mathbf{p}} \epsilon_j(\mathbf{p}) = \begin{pmatrix} \nabla_{\mathbf{p}} \epsilon_{u,j}^{\mathrm{T}} \\ \nabla_{\mathbf{p}} \epsilon_{v,j}^{\mathrm{T}} \end{pmatrix}. \tag{4.4}$$

Derivatives of $\epsilon_{u,j}$ and $\epsilon_{v,j}$ with respect to the alignment corrections can be calculated from Eq. 4.2, if the relation between the local coordinates of the impact point $\mathbf{q_{x,j}} = (u_{x,j}, v_{x,j})$ and the alignment parameters is known. For alignment of individual sensors, this relation is illustrated in Fig. 4.5. This relation is derived in publication III, by modifying the relation between local coordinates $\mathbf{q}_{x,j}$ and global coordinates to a corrected form $\mathbf{q}^c_{x,j}$ in which the alignment corrections $\Delta\mathbf{q}_j, \Delta\mathbf{R}$ (representing $\mathbf{p}$ in the form of a three-vector and a rotation matrix) are taken into account:

$$\mathbf{q}_{x,j} = \mathbf{R}(\mathbf{r}_x - \mathbf{r}_0) \tag{4.5}$$

$$\mathbf{q}^c_{x,j} = \begin{pmatrix} u^c_{x,j} \\ v^c_{x,j} \end{pmatrix} = \Delta\mathbf{R}\mathbf{q}_{x,j} + ([\Delta\mathbf{q}_j]_3 - [\Delta\mathbf{R}\mathbf{q}_{x,j}]_3)\frac{\Delta\mathbf{R}\mathbf{R}\hat{\mathrm{s}}}{[\Delta\mathbf{R}\mathbf{R}\hat{\mathrm{s}}]_3} - \Delta\mathbf{q}_j. \tag{4.6}$$

Here $\mathbf{r}_x$ denotes the impact point of the trajectory, $\mathbf{R}$ and $\mathbf{r}_0$ the initial coordinate transformation relating local and global coordinates, $\hat{\mathrm{s}}$ is a unit vector in the direction of the track at the impact point and the subscript "3" denotes the third component of a vector.

Jacobian of Composite Alignment

The alignment of individual sensors and composite structures is identical, except that the derivatives in the Jacobian of Eq. 4.3 have to be calculated differently.

To calculate the Jacobian for individual sensors, it is necessary to know Eq. 4.6, the transformation from local to global coordinates as a function of the alignment parameters, which are given in local coordinates. Similarly, to align composite objects, one needs to know the coordinate transformation from local to global coordinates as a function of the alignment parameters. In this case, alignment parameters are not expressed in the local coordinate

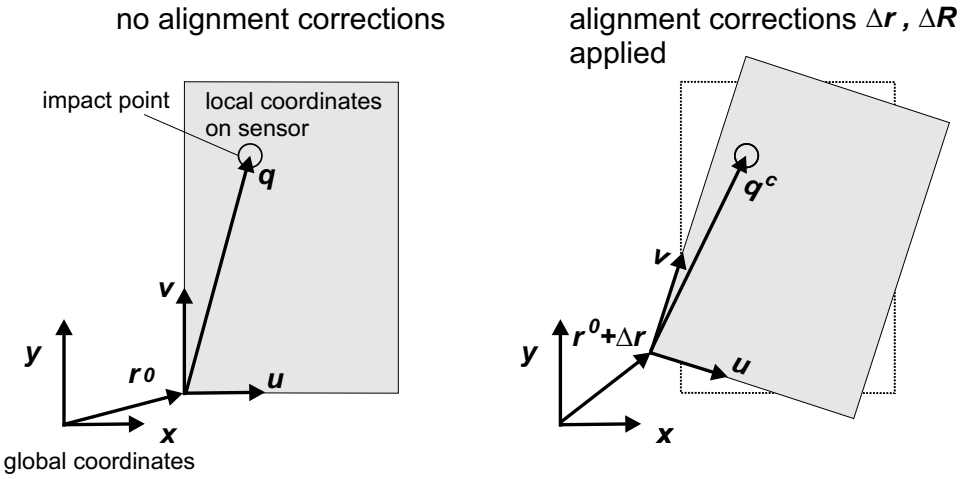

Figure 4.5: Two-dimensional illustration of the dependence of the local coordinates $\mathbf{q}$ of the impact point of the alignment corrections of the detector module. Corrections $\Delta\mathbf{r}$ and $\Delta\mathbf{R}$ are applied in the right diagram. The applied corrections are largely exaggerated.

system, but in the coordinate system of the composite object. There are thus three coordinate systems involved in the composite alignment. This coordinate transformation is illustrated in Fig. 4.6.

This result is derived in publication II, and is:

$$\mathbf{q}^c_{x,j}(\Delta\mathbf{G}, \Delta\mathbf{g}) = \mathbf{R}_C \left[\mathbf{r}_{\mathrm{x},j} - \mathbf{r}_{c,j} + h_{\mathrm{x},j}(\Delta\mathbf{G}, \Delta\mathbf{g}\hat{s}_j)\right], \tag{4.7}$$

where $\mathbf{G}$ is the rotation matrix and $\mathbf{g}$ is the three-vector of the transformation from the global to composite coordinate system. Correspondingly, $\Delta\mathbf{G}$ and $\Delta\mathbf{g}$ are the alignment corrections in the composite coordinate system. The transformation from global to local coordinate system corrected by the alignment corrections is expressed by the matrix $\mathbf{R}_C$ and three-vector $\mathbf{r}_c$. Finally, the scalar function h_x is:

$$h_\mathrm{x} = -\frac{\mathbf{R}_C(\mathbf{r}_\times - \mathbf{r}_c)\cdot\hat{\mathbf{w}}}{\mathbf{R}_C\hat{\mathbf{s}}\cdot\hat{\mathbf{w}}}. \tag{4.8}$$

Here $\hat{\mathbf{w}}$ is the unit vector along the local coordinate w.

With Eqs. 4.4 and 4.7, one can calculate the Jacobian for the composite alignment, which expresses the derivatives of the residuals with respect to the composite alignment parameters. These derivatives are given in Eqs. (9) and (10) of publication II.

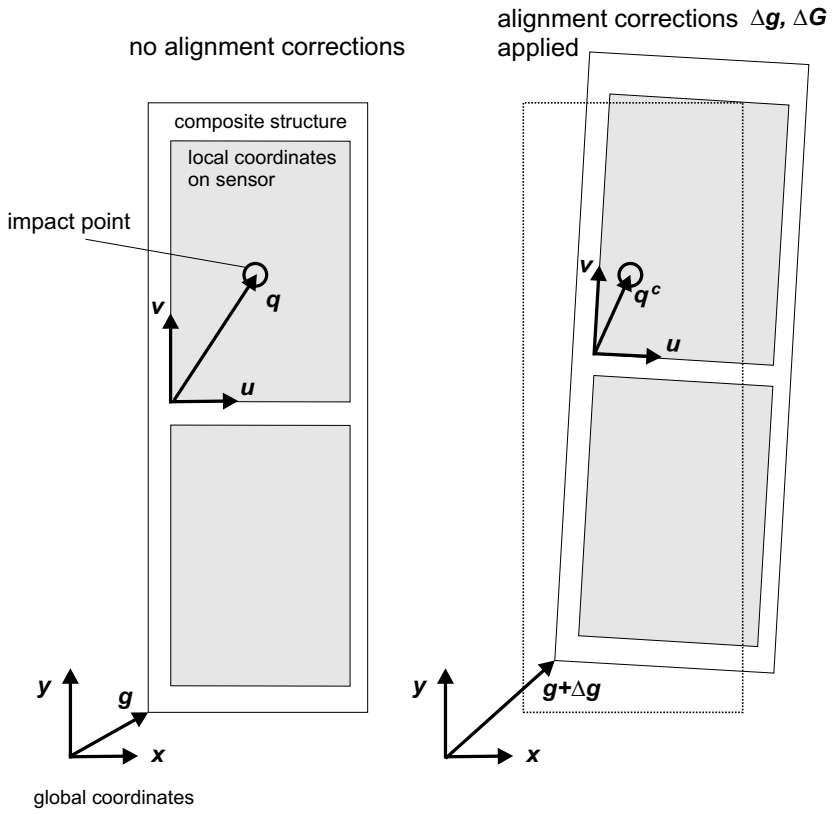

Figure 4.6: Two-dimensional illustration of the dependence of the local coordinates **q** of the impact point of the alignment corrections of the composite structure. Corrections $\Delta\mathbf{g}$ and $\Delta\mathbf{G}$ are applied in the right diagram. The applied corrections are largely exaggerated.

If the composite structure consists trivially of only one sensor, it follows that $\mathbf{G} = \mathbf{R}$, and the formalism of the composite alignment reduces to that of the alignment of individual sensors.

Another approach for calculating the derivatives for the composite alignment is the use of the chain rule

$$\frac{d\epsilon_j}{dp_k^C} = \sum_i \frac{\partial \epsilon_j}{\partial p_i} \frac{\partial p_i}{\partial p_k^C} \quad , \tag{4.9}$$

where p_k^C denotes the alignment parameter k of the composite object.

This possibility is implemented to the interface of the CMS reconstruction software ORCA in such a way that composite objects of each level of hierarchy can provide the derivatives of the alignment parameters of individual modules with respect to the derivatives of the alignment parameters of the composite object itself.

4.4 Alignment Studies of the CMS Tracker

The feasibility of the HIP algorithm has been studied for some specific cases for the CMS tracker. In particular, it has been applied to the innermost pixel detector, which is foreseen to be the first subdetector to be aligned with tracks (with the exception of the possible standalone alignment of the strip detector during the one-month pilot physics run).

The first published study using the HIP algorithm is shown in publication III, where the algorithm was used in a standalone Monte Carlo simulation of the CMS pixel barrel. Later, it was implemented within the CMS reconstruction software ORCA [39]. The ideal geometry of ORCA was misaligned with the misalignment tool presented in Chapter 5 and in publication V. Results of the alignment studies with ORCA are presented in publications II, IV, and VI.

In the most realistic study of publication VI, random misalignments were applied to individual pixel barrel modules. Misalignments in all three global coordinates were sampled from a uniform distribution in the range of $\pm 300\,\mu$m. The pixel endcaps and the CMS strip tracker were kept in their ideal positions in this study.

Muon tracks from $Z^0 \rightarrow \mu^+\mu^-$ events were utilized. To avoid a bias originating from the possibly misaligned strip tracker, track fitting was carried out in two parts. At first, the p_{T} values and the common vertex position of the two muon tracks were reconstructed by fitting tracks to hits from the pixel and the strip tracker. Then, the p_{T} values and the vertex position were utilized as constraints, and tracks were refitted with pixel hits only. With this approach, alignment of the pixel detector could be carried out even with a misaligned strip tracker. The use of the p_{T} constraint from the full track fit improved significantly the convergence of the standalone pixel alignment.

Half a million fully simulated and reconstructed $Z^0 \rightarrow \mu^+\mu^-$ events were used with 19 iterations. The result is shown in Fig. 4.7. The alignment corrections have been obtained only for 504 pixel barrel modules (720 in total), since tracks are required to have a hit in each of the three pixel barrel layers. This rejects tracks with $|\eta| \gtrsim 1.6$, and pixel barrel modules with larger $|\eta|$ cannot be aligned with tracks arriving from the interaction point. Distributions concerning global x and y should be statistically equivalent. One pixel barrel module was kept fixed to avoid shifts and to reduce deformations of the entire pixel barrel.

A good convergence is obtained for the alignment parameters. The residual RMS values are around 25 μm for all three coordinates. Although this is not yet a sufficiently precise result considering the intrinsic resolution of the pixel modules, it demonstrates that the method for the standalone alignment of the pixel detector works. The precision of the alignment can be improved by making use of a larger track sample. Also, a more diverse track sample would be beneficial in reducing global distortions, as explained in Chapter 4.2.

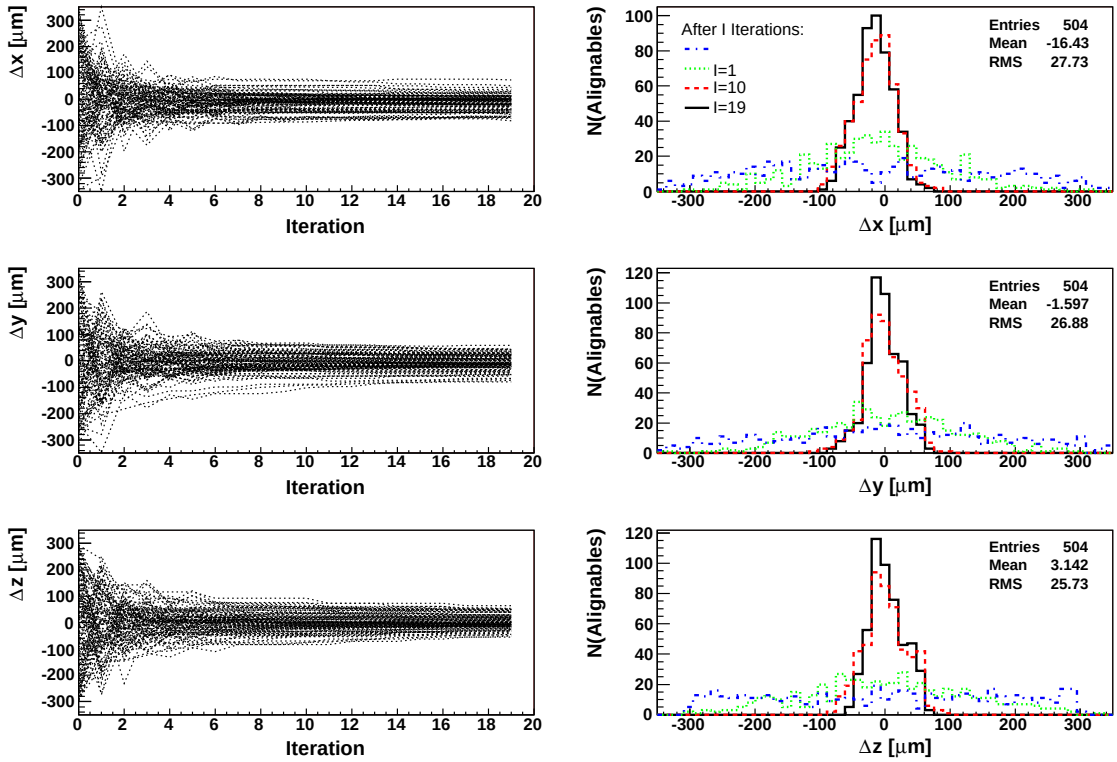

Figure 4.7: Left: convergence of alignment of 100/504 randomly selected pixel barrel modules. The residuals in global coordinates are shown as a function of the iteration number. Right: the corresponding residual distributions for all 504 modules. The residuals in global coordinates are shown for the initial misalignment (iteration 0) and after 1,10 and 19 iterations. The statistical parameters refer to the iteration 19.

4.5 Alignment of the Cosmic Rack

The applicability of the HIP algorithm was tested with test-beam data recorded with the CERN Cosmic Rack [41], a test setup that mimics a slice of the outer barrel (the TOB) of the CMS tracker. This study is presented in detail in publication IV.

The Cosmic Rack is a setup in which genuine CMS detector modules are operated to detect cosmic muons. It can also be placed in a test-beam. The Cosmic Rack, illustrated in Fig. 4.8, consists of 10 layers, which can hold two TOB rods each (carbon fibre structures holding the detector modules). Each TOB rod can host six modules measuring only one coordinate (the r-ϕ modules) or 12 modules arranged in six pairs measuring both coordinates (the stereo modules).

The Cosmic Rack was positioned in a test-beam at CERN in September 2004. It recorded data in a 120 GeV pion and 70–120 GeV muon beam. It was equipped with 48 silicon strip

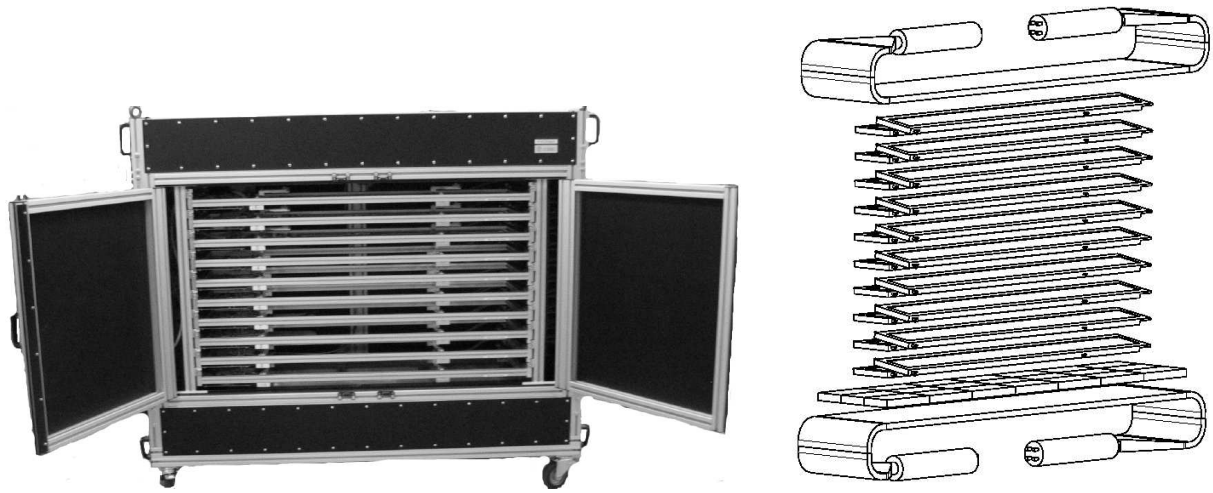

Figure 4.8: Left: Photograph of the TOB Cosmic Rack (courtesy T. Mäenpää); Right: Schematic view of rods and scintillators in the fully equipped Cosmic Rack (courtesy E. Anttila). The width of the apparatus is approximately 2 metres.

modules on six TOB rods. The two outermost rods were equipped with stereo modules, and four rods with r-ϕ modules only, as illustrated in Fig. 4.9. Two alignment parameters were considered, the coordinate of the accurate measurement (x) and the rotation around the normal of the detector module (γ angle).

The beam size of the test beam was about 8x5 mm^2 for the pion beam, and the acceptance region for the much larger muon beam was constrained by the trigger scintillator size of about 10x10 cm^2. The setup was adjusted with respect to the beam such that the beam hit the overlap region between two adjacent modules.

Two kinds of reverse-biased, AC-coupled strip sensors with a pitch of 122 and 183 μm were used, corresponding to binary resolutions of 35 or 53 μm. They consist of n-type bulk material with a p^+ implantation on the front side, manufactured from a single wafer with <100> orientation using 6" technology. Identical modules will also be utilized in the TOB.

No external measurement was used for the positions of rods (such as the LAS for CMS), and therefore the outermost rods, which were equipped with stereo modules, were not aligned but fixed to their nominal positions. This ensured that no global distortions were possible, which was an important issue for comparing results of different algorithms.

Alignment was carried out for modules of the four innermost rods. The track parameters were fitted to the reference layers only. The standard CMS reconstruction software ORCA was utilized with some modifications due to the test setup geometry. Except for these minor modifications, a full chain of genuine CMS readout hardware and reconstruction software was used.

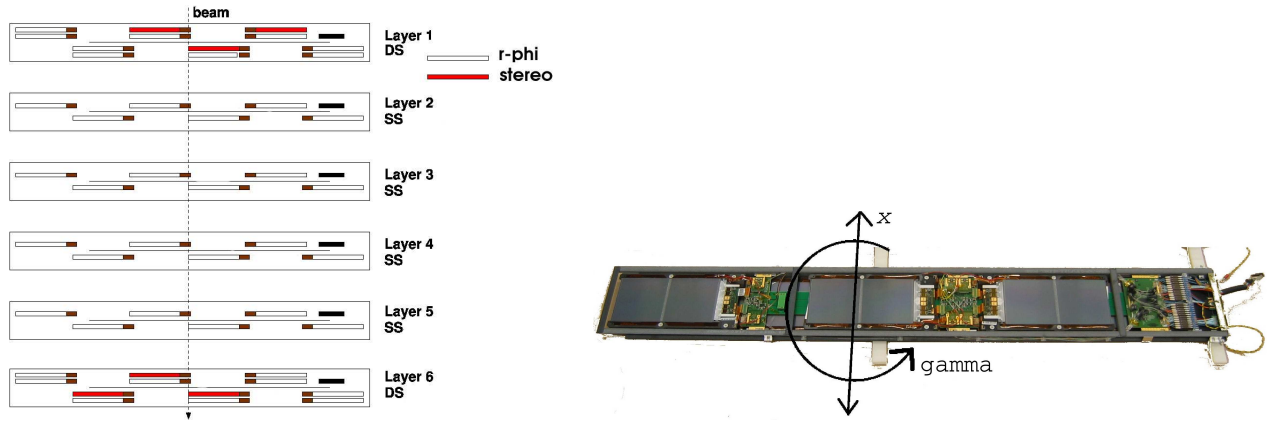

Figure 4.9: Left: Layout of the Cosmic Rack as in the test-beam of September 2004. Rod numbering is equal to layer numbering. Rods capable of holding stereo modules, which both measure x and y, are marked with DS (double sided), whereas rods holding modules that measure only one coordinate are marked as SS (single sided). Right: Rod with the x coordinate and the γ angle, which were the parameters to be aligned.

No magnetic field was used in the test-beam, and therefore tracks were fitted as straight lines. This facilitated alignment, since otherwise the initial knowledge of the momentum of particles should have been used as a constraint for track curvature. Rather strict criteria were applied in the pattern recognition and track reconstruction to avoid false tracks, which can significantly disturb the alignment process.

Alignment of the Cosmic Rack was first carried out manually with the help of residual plots. For each individual detector module, the position of the peak in the residual plot was located and the module was aligned with a corresponding x correction. Track reconstruction was repeated and new corrections were defined from the new residual plots, and these iterations were continued as long as the peak positions of the residual plots deviated more than $3\,\mu$m from zero. For simple telescope setups, this is a sufficient and straightforward way to manually align the device in x. The results of the manual alignment were compared with those obtained with more sophisticated track-based alignment methods.

The HIP algorithm was applied to the pion data measured by the Cosmic Rack. The test-beam was highly collimated with an angular spread well below 0.5 mrad. With tracks of this kind the residuals of Eq. 4.2 are, in practice, sensitive only to two alignment parameters, x and γ; it is not reasonable to try to correct the four other parameters.

Two alignment procedures were performed. In the first case, only x was aligned. In the second case, both the γ angle and x were aligned simultaneously. The centre of rotation for the γ angle was in the middle of the sensor, not coinciding with the beam. These two approaches are called HIP 1D and HIP 2D, respectively. Initial placement uncertainties were rather small, less than a mm for x and less than a milliradian for γ.

Some of the residual plots obtained with the HIP algorithm, as well as the residual distributions with a non-aligned setup, are shown in Figure 4.10. It can be seen that, for detector 3, the amount of hits associated with tracks is more than six times larger when the system is aligned, whereas for detector 4, the amount of hits quadruples with alignment. It can also be seen that, with alignment, the distributions become more Gaussian.

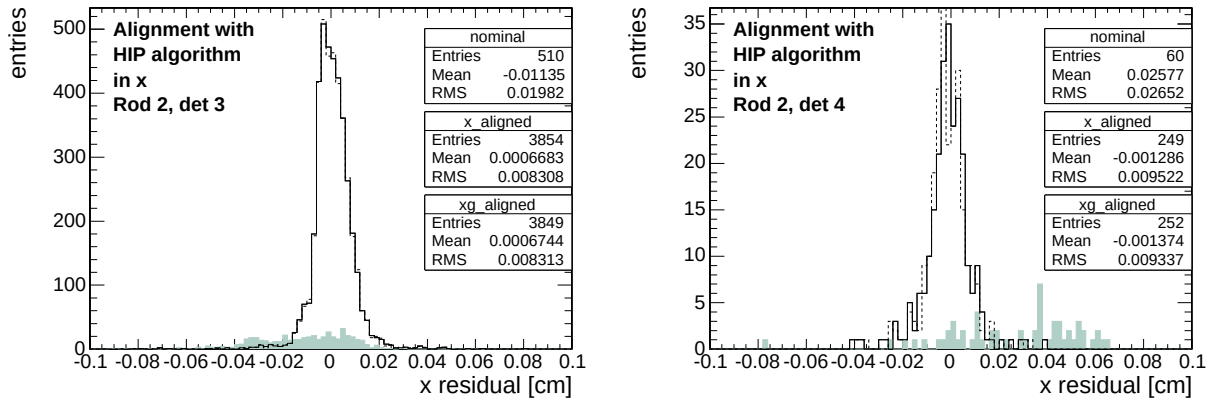

Figure 4.10: Residuals for the two modules of rod 2 before alignment (shaded colour) and after alignment with HIP 1D (solid line) and HIP 2D (dotted line). Residual distributions are very similar in both aligned cases. Pions mainly hit detector 3, while detector 4 has far fewer hits.

The exact results of the manual alignment, alignment of HIP 1D and HIP 2D, as well as the results obtained by the Millepede algorithm are presented in publication IV. All results are compatible with each other, and also the obtained mean χ^2 value of the tracks are close to each other. The manual alignment results in a slightly larger χ^2 than the HIP and Millepede methods.

The convergence of the mean χ^2 values of tracks and of some alignment parameters are shown in Figs. 4.11 and 4.12 for the methods HIP 1D and HIP 2D. The χ^2 values converge almost fully in 2–3 iterations, and the individual corrections in 3–4 iterations. However, there are small improvements in the χ^2 until iterations 9–10. The small oscillations in Fig. 4.12 are not the result of a global distortion, but due to the fact that some tracks are accepted and rejected in consecutive iterations. The number of reconstructed tracks oscillates between values of 4 113 and 4 115. Proper convergence would be obtained if the reconstructed track sample did not change.

The results obtained from the application of the HIP algorithm to the test-beam data measured by the Cosmic Rack demonstrate that the algorithm and all related parts of the ORCA reconstruction software function properly in this small testbed. The alignment corrections converge to reasonable values (with the exception of the small oscillations caused by changes in the track samples). These results represent the first application of a track-based alignment procedure on real data measured with genuine CMS hardware.

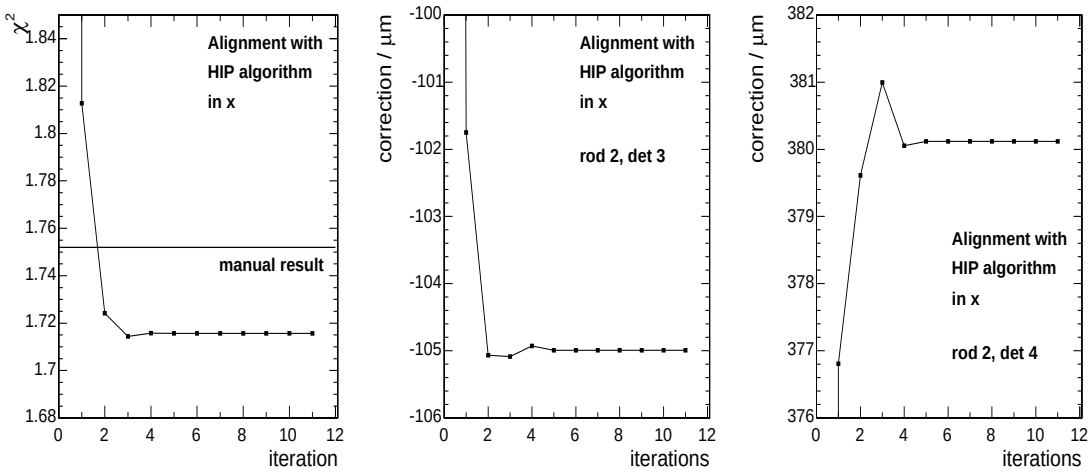

Figure 4.11: The left plot shows the convergence of the mean χ^2 value of the tracks when only x is aligned. The initial value of 61 at iteration zero is not shown. The algorithm converges to a value of 1.72. The manual corrections give a corresponding χ^2 value of 1.75 (horizontal line). The middle and the rightmost plots show the corresponding convergence of the two modules in rod 2 in x (initial value 0 not shown).

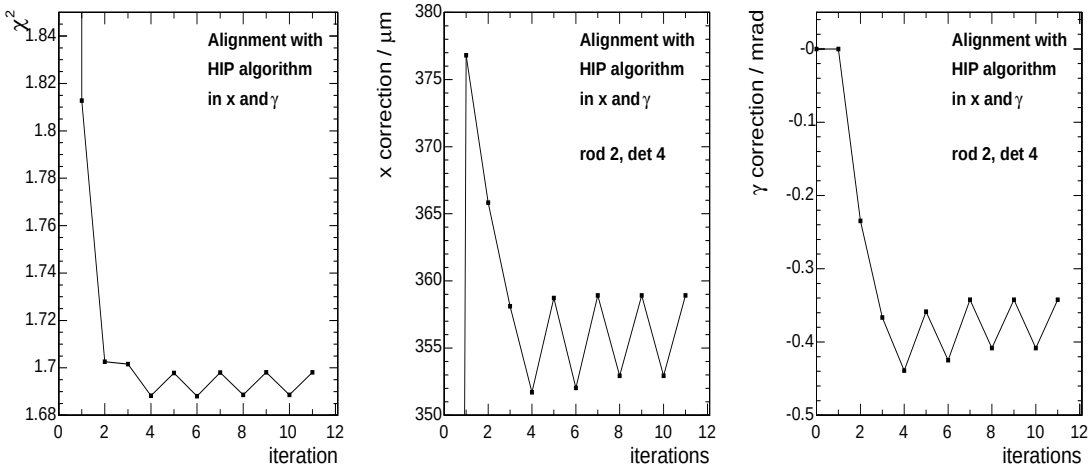

Figure 4.12: The left plot shows the convergence of the mean χ^2 of the tracks, when x and γ are aligned simultaneously (with the exception that during the first iteration γ is kept fixed). The initial value at iteration zero is not shown. The algorithm converges to a value of χ^2=1.69. The plots in the middle and on the right show the corresponding convergence of a particular module in x and γ, respectively (initial correction of 0 not shown for x). The algorithm converges, apart from the small oscillations caused by changes in the track sample.

5 Misalignment Simulation of the CMS Detector

Misalignments are among the largest potential sources of tracking uncertainties in the CMS detector. Estimates of the various installation misalignments of the CMS detector are collected and presented in publication V. Another important source of alignment uncertainties are the time-dependent effects, which are not addressed in this study. Time-dependent effects can arise from, for example, changes related to magnetic field, temperature, humidity, aging of the support structures, deformations of the cavern floor, and even seismic effects.

To assess the impact of misalignment effects on the track reconstruction and physics results, a consistent set of software tools for displacements and rotations was needed for all tracking devices in CMS. These tools simulate as closely as possible the alignment uncertainties expected during the data taking for all the tracking devices of CMS — the pixel detector, the strip tracker and the muon chambers (DTs and CSCs). The combination of this technical functionality and realistic estimates of alignment uncertainties is implemented in the CMS reconstruction software as a *misalignment scenario*.

In a large collaborative effort like the CMS experiment, it is necessary to establish common software tools with which the physics simulation and analyses can be carried out. In the field of alignment, this signifies the need for established and easy-to-use misalignment scenarios. Their use guarantees the comparability of different physics analyses.

Misalignment simulation is implemented in the reconstruction software ORCA rather than in the detector response simulation software OSCAR [42], which utilizes the ideal CMS geometry. This approach allows the end user to modify the geometry, and avoids the need to produce several datasets with different misalignments. Geometrical shifts of hits can be adequately simulated in this way, but the rare occurrence of a missed hit due to geometrical misalignment is not implemented. It is important to note that the expected geometrical mounting uncertainties do not endanger overlaps of detectors, which can provide an efficient constraint for alignment.

Two ready-made *misalignment scenarios* were implemented in the reconstruction software ORCA. The geometry files used in ORCA for the simulation of CMS contain individual sensors in their ideal positions. These positions have to be relocated (misaligned) before any alignment studies can be made. Misaligned geometry also allows studies of the sensitivity of physics variables and detector performance to the misalignments. Misalignment scenarios apply realistic misalignment to individual sensors, as well as to composite objects of different levels of hierarchy. This hierarchy, as implemented in the reconstruction software, is shown in Fig. 4.4.

5.1 Development of Misalignments

During the assembly of the CMS tracker, positions and orientations of the tracker detector components are measured and stored in databases. Measurements are carried out with, for example, photogrammetry or contact coordinate measurement machines. For instance, the manufacturing of the TOB rods were carried out in Finland, and all 753 rods were measured in a Zeiss 3D coordinate measurement machine, as explained in publication IV. Results of these measurements are saved in a database, and used as corrections to the ideal tracker geometry. For some other structural parts of the tracker, only a sample is measured. In this case, the standard deviation of the measurements is used as an estimate of the corresponding mounting uncertainty, and this error is taken into account in the initial track reconstruction.

The estimated mounting precision of individual sensors in the tracker are shown in Table 5.1. For comparison, the sensor resolutions are also presented. For all tracker parts, the intrinsic sensor resolution is better than the mounting precision.

Table 5.1: Mounting precisions in μm for individual tracker sensors, as well as for their support structures for pixel barrel (TPB), inner barrel (TIB), outer barrel (TOB), pixel endcaps (TPE), inner discs (TID) and endcaps (TEC). Characteristics of corresponding sensors are also presented. Resolutions are binary resolutions, except for TPB and TPE, which are from Ref. [43]. The less precise resolution of stereo strip modules is not presented.

	TPB	TIB	TOB	TPE	TID	TEC
Modules	130	200	100	25	105	50
Ladders, Rods, Rings or Petals	50	200	100	50	300	100
Pixel size	100×150			100×150		
Strip pitch		81/118	122/183		97–143	96–183
Resolution	10–20	23/34	35/52	10–20	28–41	28–53

Mounting uncertainties of the order of 100–500 μm also exist for higher level support structures of the tracker such as layers, discs and barrels. These uncertainties are already reduced before the first data taking by the information provided by the laser alignment system (LAS). The pixel detector and the TID are out of the reach of the LAS, and therefore their initial placement uncertainties are directly determined by manufacturing and installation processes. For the muon system, uncertainties of several mm are expected due to displacements caused by the magnetic forces, but can be reduced by the muon hardware alignment system.

5.2 Misalignment Scenarios

To follow the expected evolution of the performance of the different alignment procedures, several scenarios were developed and described in publication V. The first scenario is

supposed to describe the conditions expected at the initial stage of the data taking (*First Data* scenario), while the second one addresses the alignment uncertainties expected when the full alignment of the detector is done (*Long Term* scenario). In addition, the *Survey Only* scenario was provided for specific needs of the muon system. All physics studies are intended to be carried out with *First Data* or *Long Term* scenarios.

For the *First Data* scenario, the initial mounting precisions play an important role. They are improved by the LAS measurements, and also the by the very first results with TBA. The amount of data at this stage, a few hundred pb^{-1}, is probably sufficient to fully align the pixel detector. However, with these data, only the higher level structures of the strip detector, such as the barrel layers, can be aligned. It is estimated that, for the pixel detector, the initial mechanical constrains can be improved by TBA to correspond to a Gaussian distribution with an RMS smaller by an order of a magnitude (giving, for instance, RMS of 10 μm for TPB and 5 μm for TPE in each direction). For the *Long Term* scenario, the amount of data is sufficient to also carry out full alignment for the strip detector. Also, in this case, the RMS is assumed to improve by an order of magnitude.

These uncertainties are presented in Table 5.2. In the misalignment scenarios, misalignments for sensor and layer/disc level structures are independent random variables sampled from the corresponding distributions. Details of calculations and references are given in publication V.

Table 5.2: Placement uncertainties for layer/disc-level structures for Δx, Δy, Δz and R_z (rotation around the local axis corresponding to the beam direction). Corrections provided by Laser Alignment is taken into account. For the pixel parts and the TID, for which LAS is not available, the range of the uniform distribution is given. Assumptions of applicability of TBA in the two scenarios are also presented.

	Δx [μm]	Δy [μm]	Δz [μm]	R_z [μrad]	LAS available	TBA assumed in *First Data*	TBA assumed in *Long Term*
TPB	$\pm$100	$\pm$100	$\pm$100	$\pm$100	no	yes	yes
TIB	105	105	500	90	yes	no	yes
TOB	67	67	500	59	yes	no	yes
TPE	$\pm$50	$\pm$ 50	$\pm$ 50	$\pm$50	no	yes	yes
TID	$\pm$400	$\pm$400	$\pm$400	$\pm$100	no	no	yes
TEC	57	57	500	46	yes	no	yes

The scenarios are based on the best current estimates, which will be refined (perhaps even significantly) as time evolves and can only be considered as a snapshot of our current understanding of misalignment effects.

The transition from one scenario to another is not clearly defined, and also depends on success in the operation of the LHC machine. For the tracker, it is expected that the limiting factor in the alignment accuracy is the amount of integrated luminosity. If minimum bias events prove to be useful, they are available abundantly, but further studies are still needed. For the muon system, it is expected that alignment accuracy follows a learning

curve that is not limited by the integrated luminosity, but by experience and understanding of the behaviour of the device.

The *First Data* situation should be achieved after a short time of data taking (a couple of weeks or a month) of the First Physics run. As more data is collected, alignment progressively reaches the *Long Term* case. The expected amount of integrated luminosity after one month of data taking in the First Physics run is about 100 pb^{-1}, and the current, rather uncertain, estimate for the integrated luminosity reached during the 6-month period of the First Physics run is 1 fb^{-1} [5]. It is possible (although uncertain) that the amount of integrated luminosity of the First Physics run is sufficient to reach the *Long Term* scenario. The uncertainty especially concerns the tracker, which is more dependent on the amount of data than the muon system. These values, as well as estimates for the corresponding integrated luminosities, are presented in Table 5.3.

Table 5.3: Scenarios in terms of time from the beginning of operation, as well as in terms of estimated integrated luminosity. These numbers are estimates only, based on the expected luminosity evolution of Chapter 2.2.

Scenario	Run time	Integrated luminosity
Survey Only	0–1 month	0–100 pb^{-1}
First Data	1 month–6 months	100 pb^{-1}–1 fb^{-1}
Long Term	6 months–10 years	1 fb^{-1}–500 fb^{-1}

To analyze the physics performance of the CMS detector, the scenarios have been used in the various physics analyses in [7, 5]. They have also been utilized in the performance studies of the different alignment algorithms.

5.3 Effects of Misalignment

The misalignment scenarios enable easy-to-use studies of physics results with misaligned detector geometry, and have been an essential ingredient in the analyses carried out within the CMS collaboration. The effects of misalignment on track and vertex reconstruction is discussed in detail in, for instance, Ref. [44].

An important feature of the misalignment scenarios is the possibility of setting the *Alignment Position Error* (APE), illustrated in Fig. 5.1. It is a variable for each detector module, which characterizes the measurement uncertainty of a given detector due to misalignment. The APE is combined with the spatial (intrinsic) resolution of the device giving the total error of the position of hits belonging to these detector modules.

The APE can be set by the user. Its value has a direct impact on the performance of the track reconstruction efficiency, fake rate and momentum resolution. The choice of an optimal value of APE is discussed in publication V.

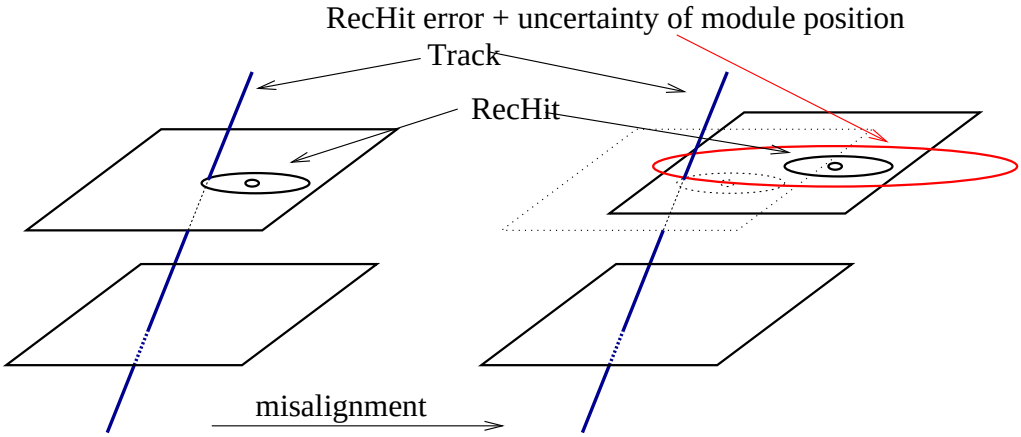

Figure 5.1: Alignment Position Error. Track fit with an ideally positioned and misaligned sensor is shown. The displacement is added to the errors of the reconstructed hit (RecHit).

Figure 5.2 shows the track-finding efficiency of the tracker as a function of the pseudorapidity when only the TOB and TIB rods and the pixel endcap blades are misaligned (dashed line), and also when the pixel ladders in addition are misaligned (solid line). Misalignments were sampled from a Gaussian distribution with an RMS of 100 μm[7]. Single muon tracks are used. No correlated effects (e.g. misalignments of a higher level object like TOB barrels) were taken into account in this study. The APE, which affects the search window of pattern recognition in track finding, is not taken into account in the reconstruction algorithm used for the left plot. With the ideally-aligned pixel detector, the track-finding efficiency is near to 1 up to $|\eta| = 2.0$. When the pixel detector is also misaligned, the efficiency drops below 0.8 in this region. In the right plot, the APE is taken correctly into account. In this case, full efficiency is recovered.

Figure 5.3 shows the impact of the muon APEs on the efficiency and p_{T} resolution for the full (tracker and muon detectors) reconstruction of the muons. We are here in a situation different from that in the tracker: muon APEs hardly affect the efficiency, but significantly improve the muon momentum resolution. Muon track reconstruction uses two approaches, one in which trajectory seeding takes place in the muon detectors, and is extrapolated to the outer tracker surface, and one in which tracks reconstructed in the tracker are extrapolated to the muon detector to identify the muon. Efficiency is therefore insensitive to misalignment of the muon system in the presence of an ideally aligned tracker, since muon tracks can be reconstructed in the tracker, and identified as muons even with hit information from individual layers of the muon detectors. However, the muon momentum resolution is affected by the misaligned muon system, especially if the alignment position error is not properly taken into account.

[7]In publication V, an incorrect RMS of 10 μm is stated. These results have now been reproduced with more data and also with a more appropriate way of calculating the errors. The latest version of the reconstruction software ORCA was also used.

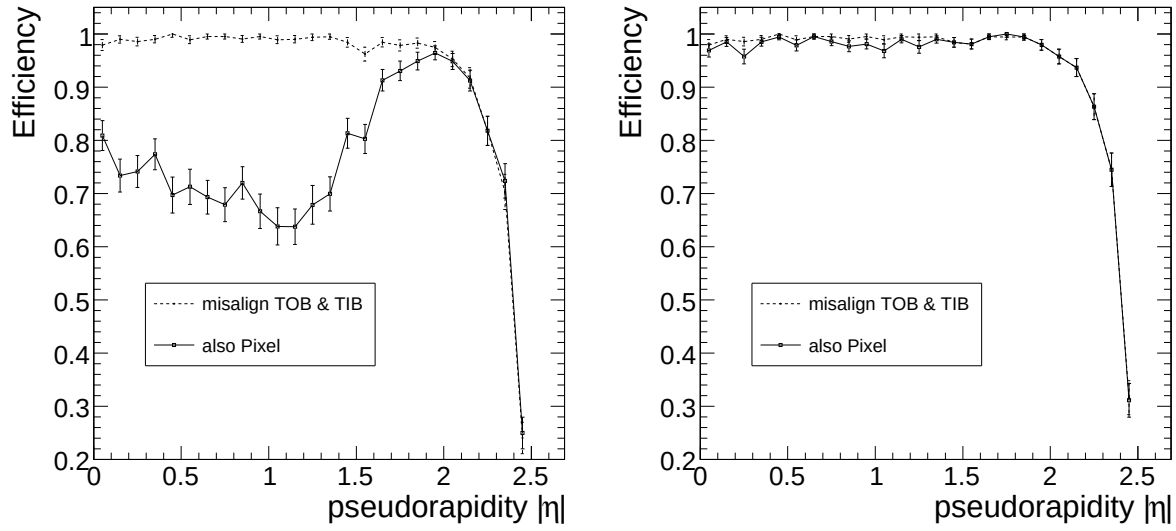

Figure 5.2: Track-finding efficiency as a function of the pseudorapidity η, for the misaligned TOB and TIB (dashed line), and for the misaligned TOB, TIB and pixel detector (solid line). Left: the APE is not taken into account; Right: the APE is taken into account.

Figures 5.4, 5.5 and 5.6 show the η dependence of the $1/p_{\mathrm{T}}$ resolution obtained by the full track reconstruction (including the tracker and the muon system) in the case of misalignments applied to tracker, muon, or both. Single muons with transverse momenta p_{T} of $100\,\mathrm{GeV}/c$ and $1\,\mathrm{TeV}/c$ were used. It can be seen that misalignment of the muon system has a significant effect only for high-p_{T} muons, and that alignment of the tracker is important for the muon momentum resolution for muons with $p_{\mathrm{T}} = 100\,\mathrm{GeV}/c$ and below.

More examples illustrating the effects of misalignments on physics variables can be found in Refs. [44, 7] and in Ref. [5], where the misalignment scenarios have been systematically used in the performance studies of the CMS detector. For instance, it was found for a light supersymmetric Higgs boson (h^0) that the signal selection efficiency for the *Long Term* misalignment scenario is reduced by $\sim 10\%$, whereas in the case of the *First Data* misalignment scenario the reduction was $\sim 17\%$ (compared to the ideal geometry), and that no effect on the position or width of the Higgs mass peak was observed [5].

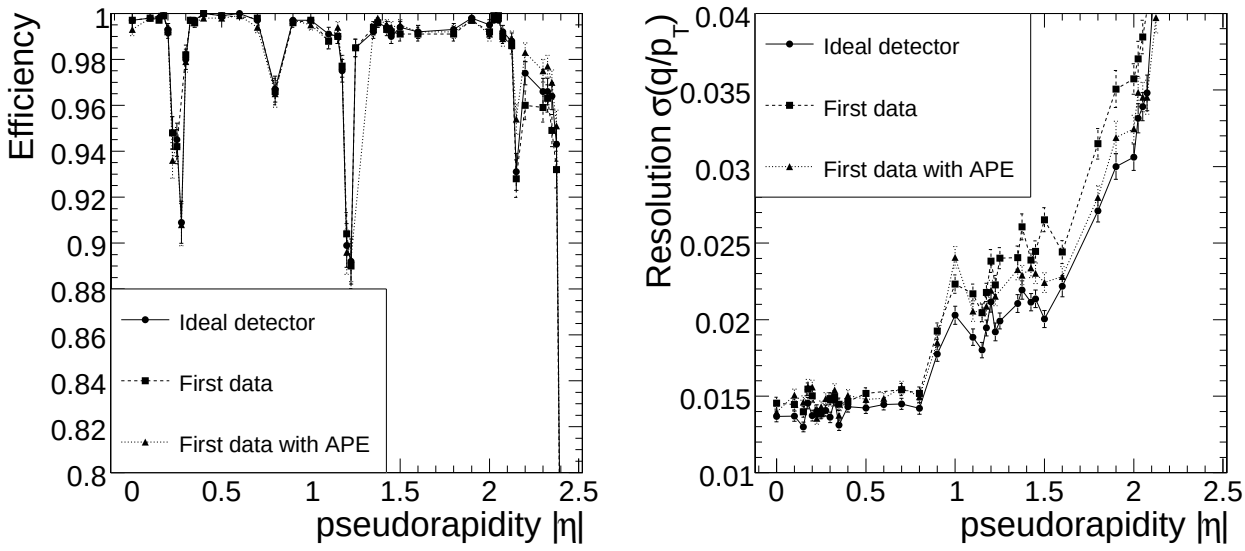

Figure 5.3: Muon reconstruction efficiency (left) and $1/p_{\mathrm{T}}$ resolution (right) as a function of the pseudorapidity η for muons with a generated p_{T} of 100 GeV/c, for the ideal alignment and for the *First Data* scenario with and without the muon APE. The nominal geometry of the tracker is used in all three cases.

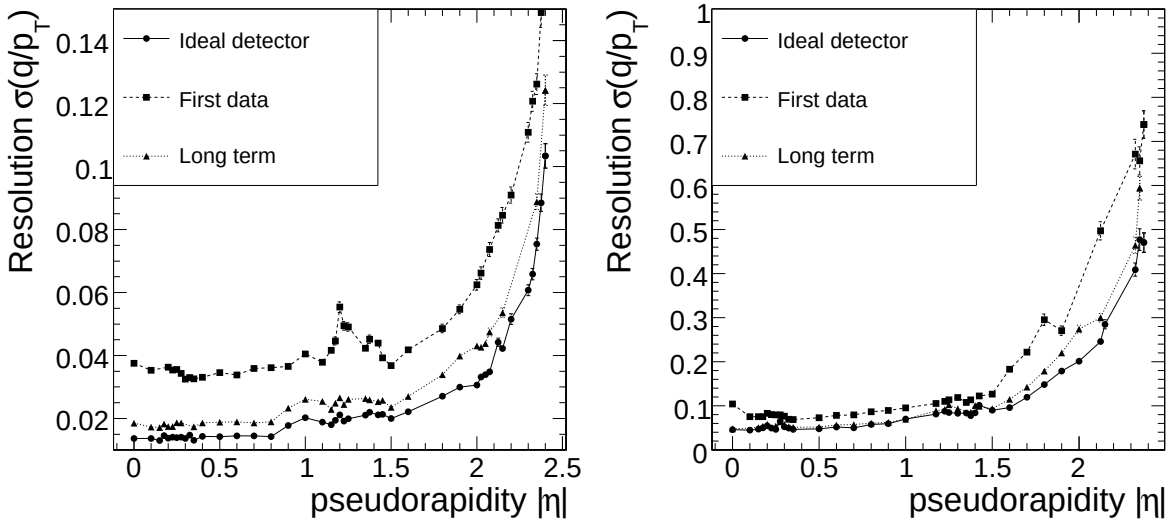

Figure 5.4: Muon $1/p_{\mathrm{T}}$ resolution (sigma of a Gaussian fit) as a function of η for the ideal alignment and for the *First Data* and *Long Term* tracker misalignment scenarios, for $p_{\mathrm{T}}^{\mathrm{gen}} = 100\,\mathrm{GeV}/c$ (left) and $p_{\mathrm{T}}^{\mathrm{gen}} = 1\,\mathrm{TeV}/c$ (right).

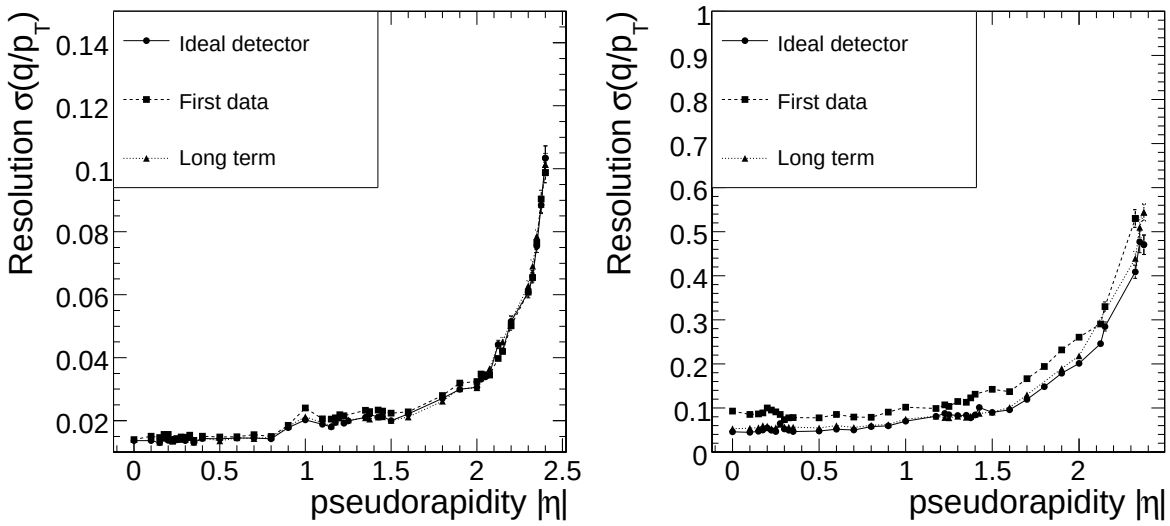

Figure 5.5: Muon $1/p_{\mathrm{T}}$ resolution (sigma of a Gaussian fit) as a function of η for the ideal alignment and for the *First Data* and *Long Term* muon misalignment scenarios, for $p_{\mathrm{T}}^{\mathrm{gen}} = 100\,\mathrm{GeV}/c$ (left) and $p_{\mathrm{T}}^{\mathrm{gen}} = 1\,\mathrm{TeV}/c$ (right).

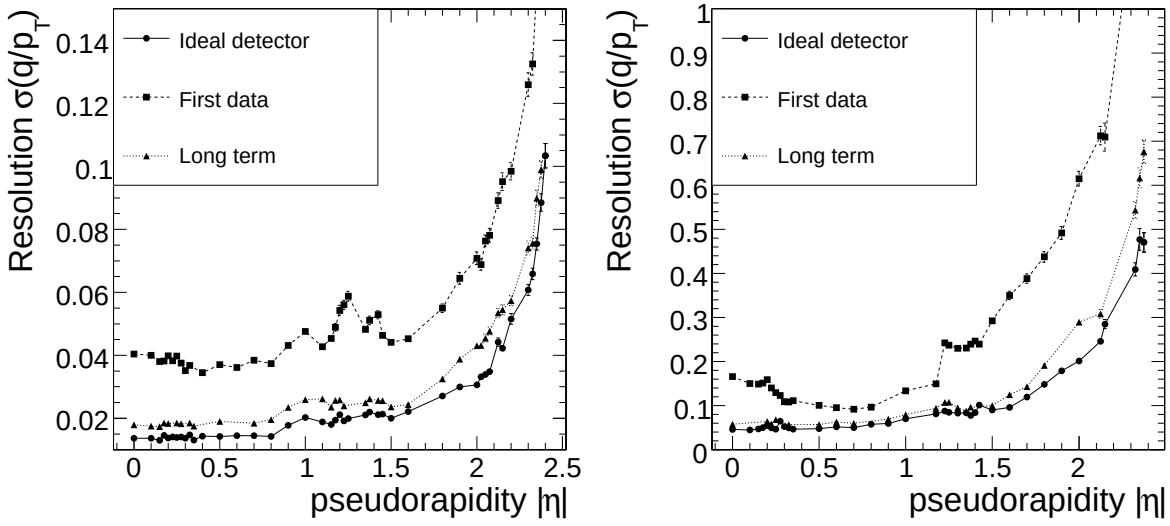

Figure 5.6: Muon $1/p_{\mathrm{T}}$ resolution (sigma of a Gaussian fit) as a function of η for the ideal alignment and for the *First Data* and *Long Term* scenarios applied simultaneously to the tracker and to the muon detector, for $p_{\mathrm{T}}^{\mathrm{gen}} = 100\,\mathrm{GeV}/c$ (left) and $p_{\mathrm{T}}^{\mathrm{gen}} = 1\,\mathrm{TeV}/c$ (right).

6 Conclusions

The purpose of this work was to develop and evaluate a track-based alignment algorithm envisaged for the pixel detector of the CMS experiment at CERN. The algorithm, known as the Hits and Impact Points (HIP) algorithm, was first used in a standalone simulation of the CMS pixel barrel, and later within the CMS reconstruction software ORCA with simulated data. The algorithm and the ORCA software was applied to test-beam data recorded with the CMS TOB Cosmic Rack.

The simulation studies with half a million $Z^0 \rightarrow \mu^+\mu^-$ events show that alignment uncertainties can be reduced down to a level of $25\,\mu$m. This demonstrates that the method for the standalone alignment of the pixel detector works. Detailed and realistic studies with more diverse data samples are necessary to reach the objective, which is to decrease alignment uncertainties down to a level comparable to the intrinsic sensor resolution.

The alignment studies with the Cosmic Rack show that the HIP algorithm and the reconstruction software ORCA perform well with the CMS readout hardware. Successful alignment is well illustrated by the multiple increase in the number of reconstructed tracks after the alignment was carried out. Alignment parameters obtained with the HIP algorithm were compared to results obtained with the Millepede algorithm and manually obtained results. All results were compatible.

The studies of the alignment algorithm involve a thorough understanding of the expected placement uncertainties, as well as their appropriate simulation. The initial uncertainties were estimated and ready-made *misalignment scenarios* were implemented. These scenarios are used as a basis for track-based alignment studies, and they can also be used in the realistic simulation of misalignments. These scenarios have become one of the *de facto* standard validation tools for the physics performance of the CMS detector, and will also be utilized in future alignment studies.

References

[1] CMS Collaboration, *CMS Technical Proposal*, CERN/LHCC 94-38 (1994).

[2] ATLAS Collaboration, *ATLAS Technical Proposal*, CERN/LHCC 94-43 (1994).

[3] TOTEM Collaboration, *TOTEM Technical Design Report*, CERN-LHCC-2004-002 (2004).

[4] The LEP Collaborations and the LEP Electroweak Working Group, *A Combination of Preliminary Electroweak Measurements and Constraints on the Standard Model* LEPEWWG/2006/01 [arXiv:hep-ex/0612034] (2006).

[5] CMS Collaboration, *CMS Physics Technical Design Report Volume II: Physics Performance*, CERN/LHCC 2006-021 (2006).

[6] ATLAS Collaboration, *ATLAS Detector and Physics Performance Technical Design Report Volume II*, CERN/LHCC 99-15 (1999).

[7] CMS Collaboration, *CMS Physics Technical Design Report Volume I: Detector Performance and Software*, CERN/LHCC 2006-001 (2006).

[8] R. Bailey, *Beam Commissioning Procedure - Overall strategy for early luminosity operation with protons*, Large Hadron Collider project LHC-OP-BCP-0001 rev 1.0 (2004).

[9] CMS Collaboration, *CMS Tracker Technical Design Report*, CERN/LHCC 98–6 (1998).

[10] P. Billoir, *Progressive track recognition with a Kalman-like fitting procedure*, Computer Physics Communications 57:390–394 (1989).

[11] CMS Collaboration, *CMS Muon Technical Design Report*, CERN-LHCC 97-31 (1998).

[12] CMS Collaboration, *CMS Magnet Technical Design Report*, CERN LHCC 97-10 (1997).

[13] V. Blobel, *Software alignment for tracking detectors*, Nucl. Instr. and Meth. A 566:5–13 (2006).

[14] B. Mours et al., *The design, construction and performance of the ALEPH Tracking Detectors*, Nucl. Instr. and Meth. A 453:101–115 (1996).

[15] A. Bonissent and D. Rousseau, *Alignment of the upgraded VDET at LEP2*, ALEPH 97-116 MINIV 97-005 (1997).

[16] A. Andreazza and E. Piotto, *The Alignment of the DELPHI Tracking Detectors*, DELPHI 99-153 TRACK 94 (1999).

[17] P. Brückman de Renstrom, *The Final Alignment of the Barrel Silicon Tracker at LEP2*, DELPHI 2004-047 TRACK 098 24 pp. (2004).

[18] K. Österberg, *Performance of the vertex detectors at LEP2*, Nucl. Instr. and Meth. A 435:1–8 (1999).

[19] K. Abe et al., *Design and performance of the SLD vertex detector, a 307 Mpixel tracking system*, Nucl. Instr. and Meth. A 400:287–343 (1997).

[20] D. J. Jackson, Dong Su, and F. J. Wickens, *Internal alignment of the SLD vertex detector using a matrix singular value decomposition technique*, Nucl. Instr. and Meth. A 491:287–343 (2002).

[21] V. Re et al., *The BaBar Silicon-Vertex Tracker: Performance, Running Experience, and Radiation-Damage Studies*, IEEE Trans. Nucl. Sci. 49(6):3284 – 3289 (2002).

[22] V. Blobel and C. Kleinwort, *A new method for the high-precision alignment of track detectors*, Proceedings of Conference on Advanced Statistical Techniques in Particle Physics [arXiv:hep-ex/0208021] (2002).

[23] D. Pitzl et al., *The H1 silicon vertex detector*, Nucl. Instr. and Meth. A 454:334–349 (2000).

[24] T. Kohno, *Alignment of the ZEUS micro-vertex detector using cosmic tracks*, Nucl. Instr. and Meth. A 559:153–157 (2006).

[25] C.H. Wang, F.D. Snider, J. Incandela, E. Kajfasz, P. Singh, D. Stuart, M. Wang, W. Yao, and J.C. Yun, *Alignment of SVX' Using Run 1B Data*, CDF/ANAL/SEC_VTX/CDFR/3002 (1995).

[26] R. McNulty, T. Shears, and A. Skiba, *A Procedure for Software Alignment of the CDF Silicon System*, CDF/DOC/Tracking/57000 (2001).

[27] A. Sopczak, *Alignment of the central D0 detector*, Nucl. Instr. and Meth. A 566:142–148 (2006).

[28] P. Brückman de Renstrom, *Least squares approach to the alignment of the generic high precision tracking system*, Proceedings of the PHYSTAT05 conference (2006).

[29] A. Hicheur and S. Gonzalez Sevilla, *Implementation of a global fit method for the alignment of the silicon tracker in ATLAS Athena framework*, Proceedings of the CHEP06 conference (2006).

[30] P. Schleper, G. Steinbrück, and M. Stoye, *Software Alignment of the CMS Tracker using MILLEPEDE II*, CMS Note 2006/011 12 pp. (2006).

[31] M. Karagöz Ünel, P. Brückman de Renström, K. Bemardet, and A. Hicheur, *Parallel computing studies for the alignment of the ATLAS silicon tracker*, Proceedings of the CHEP06 conference (2006).

[32] C. Eklund al., *Silicon beam telescope for CMS detector tests*, Nucl. Instr. and Meth. A 430:321–332 (1999).

[33] E. Widl, W. Adam, and R. Frühwirth, *A Kalman Filter for Track-based Alignment*, CMS Note 2006/022 (2006).

[34] R. Frühwirth, *Application of Kalman filtering to track and vertex fitting*, Nucl. Instr. and Meth. A 262:444–450 (1987).

[35] *CMS Trigger/DAQ Project Technical Design Report Volume II*, CERN-LHCC 2002-26 (2002).

[36] V. Drollinger, *Simulation of Beam Halo and Cosmic Muons*, CMS Note 2005/012 (2005).

[37] A. Heikkinen and V. Karimäki, *Fine Calibration of Detector Positions by Tracks in Helsinki Silicon Beam Telescope*, CMS Note 1999/029 (1999).

[38] K. Banzuzi et al., *Performance and calibration studies of silicon strip detectors in a test beam*, Nucl. Instr. and Meth. A 453:536–544 (2000).

[39] *CMS Reconstruction Software ORCA*, http://cmsdoc.cern.ch/orca/ (10.1.2007).

[40] P.K. MacKeown and D.J. Newman, *Computational Techniques in Physics*, Adam Hilger Ltd. (1984).

[41] T. Mäenpää, E. Hæggström, E. Anttila, A. Onnela, T. Lampén, P. Luukka, V. Karimäki, and J. Tuominiemi, *Finnish CMS-TOB cosmic rack*, Nucl. Instr. and Meth. A 570:258–261 (2007).

[42] *Object oriented Simulation for CMS Analysis and Reconstruction*, http://cmsdoc.cern.ch/oscar/ (10.1.2007).

[43] M. Atac et al., *Beam test results of the US-CMS forward pixel detector*, Nucl. Instr. and Meth. A A488:271–281 (2002).

[44] N. De Filippis et al., *Impact of Silicon Tracker Misalignment on Track and Vertex Reconstruction*, Nucl. Instr. and Meth. A 566:45–49 (2006).